Naval Research Laboratory

Washington, DC 20375-5320

NRL/MR/7228--05-8852

Addition of Vertical Velocity to a One-Dimensional Aerosol and Trace Gas Model

WILLIAM A. HOPPEL

Computational Physics Inc.
Springfield, VA

PETER CAFFREY
GLENDON M. FRICK

Remote Sensing Physics Branch
Remote Sensing Division

January 12, 2005

REPORT DOCUMENTATION PAGE

Form Approved
OMB No. 0704-0188

1. REPORT DATE *(DD-MM-YYYY)*	2. REPORT TYPE	3. DATES COVERED *(From - To)*
12-01-2005	Memorandum	October 2004-November 2004

4. TITLE AND SUBTITLE

Addition of Vertical Velocity to a One-Dimensional Aerosol and Trace Gas Model

5a. CONTRACT NUMBER

5b. GRANT NUMBER

5c. PROGRAM ELEMENT NUMBER

6. AUTHOR(S)

William A. Hoppel,* Peter Caffrey, and Glendon M. Frick

5d. PROJECT NUMBER

5e. TASK NUMBER

5f. WORK UNIT NUMBER

7. PERFORMING ORGANIZATION NAME(S) AND ADDRESS(ES)

Naval Research Laboratory, Code 7228
4555 Overlook Avenue, SW
Washington, DC 20375-5320

8. PERFORMING ORGANIZATION REPORT NUMBER

NRL/MR/7228--05-8852

9. SPONSORING / MONITORING AGENCY NAME(S) AND ADDRESS(ES)

Office of Naval Research, BCT1
800 North Quincy Street
Arlington, VA 22217-5660

10. SPONSOR / MONITOR'S ACRONYM(S)

11. SPONSOR / MONITOR'S REPORT NUMBER(S)

12. DISTRIBUTION / AVAILABILITY STATEMENT

Approved for public release; distribution is unlimited.

13. SUPPLEMENTARY NOTES

*Computational Physics Inc., Springfield, VA

14. ABSTRACT

This report describes the method used to include large-scale vertical motions, such as subsidence and lifting in the 1-D (dimensional) NRL aerosol model (MARBLES), in which all aerosol sources, sinks, and transformation processes take place within the horizontal layers defined as cells. The large-scale convergences and divergences in the wind field responsible for the vertical motion must be generated externally, such as by the Navy's 3-D mesoscale model COAMPS (Coupled Ocean Atmosphere Meteorological Prediction System). The aerosol model is run along an air-mass trajectory generated from the output of COAMPS that includes vertical profiles of meteorological data required by the aerosol model. The 1-D aerosol model can be visualized as a Lagrangian column moving with a mean horizontal wind speed. Tests are used to illustrate the performance of the model, and the conditions under which the 1-D (horizontally homogeneous) solution is valid are discussed.

15. SUBJECT TERMS

Aerosol; Model; Trajectory; Prediction; Subsidence; COAMPS

16. SECURITY CLASSIFICATION OF:			17. LIMITATION OF ABSTRACT	18. NUMBER OF PAGES	19a. NAME OF RESPONSIBLE PERSON
a. REPORT	b. ABSTRACT	c. THIS PAGE			Glendon M. Frick
Unclassified	Unclassified	Unclassified	UL	42	19b. TELEPHONE NUMBER *(include area code)* (202) 767-3589

Standard Form 298 (Rev. 8-98)
Prescribed by ANSI Std. Z39.18

CONTENTS

Addition of Vertical Velocity to a One-Dimensional Aerosol and Trace Gas Model

I. INTRODUCTION

The NRL aerosol model includes all aerosol processes believed to be important in the Marine Boundary Layer (MBL). These processes can be divided into three classes with respect to their dependence on meteorology: (1) those processes that are only incidentally dependent on meteorology, (2) those that are driven almost entirely by the meteorology and (3) those for which both the meteorology and the aerosol properties are crucial. In the first class are processes such as coagulation, diffusional growth of core material by condensation of gas-phase reaction products (such as sulfate), gravitation settling, and nucleation of new particles. These processes are determined at the molecular mean-free-path and aerosol size scales. The ambient relative humidity affects these processes indirectly through the change in aerosol size by uptake of water (for hygroscopic aerosol components). The strength of atmospheric turbulence can have a small inertial effect on coagulation. In the second class of processes, such as, horizontal advection, vertical mixing of aerosols, and exchange with the free troposphere, meteorological conditions play the dominant role. Other processes are crucially dependent on both the current meteorology and microphysical properties of the aerosol. Examples of these are the various precipitation scavenging mechanisms, addition of aerosol mass during cloud processing (liquid-phase chemistry), surface deposition and generation of sea-salt aerosol at the sea surface.

It is clear from the above that it is impossible to model the spatial and size distribution of aerosols in the MBL without having an accurate concurrent description of the meteorological fields (wind, turbulent mixing, RH, temperature, clouds and precipitation fields). The most robust and accurate aerosol models are sectional models where the aerosol size distribution is divided into a number of size sections with each section containing a number of (chemical) components. The NRL sectional model eliminates stiffness and numerical diffusion caused by calculating condensation and evaporation of water vapor during movement of the aerosol through relative humidity gradients and greatly reduces numerical diffusion for growth of core material by various gas-to-particle conversion mechanisms (Fitzgerald et al.[1998a,b] and Gelbard et al. [1998]).

The NRL (1-D aerosol model is typically run with 37 size sections (between 0.005 and 15 μm dry radius) and four components, sulfate, sea salt, an insoluble component (dust), and water in equilibrium with the soluble components at ambient RH. To fully integrate an aerosol model into a 3-D meteorological model would require carrying and calculating over 100 aerosol variables at each grid point of the model in addition to the meteorological variables. While the rapid increase in computing speed may make this possible in the future, or even the present, provided enough computing time is available, we have settled on a less ambitious model integration scheme that uses the output of a high resolution mesoscale model to drive our 1-D aerosol model.

The model integration being pursued is the following: A high-resolution mesoscale model, in our case the Navy's COAMPS model, is run over the geographical region and time of

Manuscript approved December 6, 2004.

interest and the meteorological variables at each grid point are stored at specified time intervals, typically every hour. In addition to the normal meteorological fields, some internally generated parameters, such as the turbulent mixing coefficients generated by the boundary layer parameterization used in the model, are also saved. From the horizontal wind field, a mean MBL back trajectory from any point of interest is generated. The NRL 1-D aerosol model, here considered as a vertical column, is advected along this trajectory. The metrological data required by the aerosol model is extrapolated using the grid points that lie closest to the points on the back-trajectory. Because of the well-mixed character of the MBL, the concept of a 1-D column moving with the mean wind speed in the MBL is a reasonable approximation. The extension of the column into the lower free troposphere (FT) to simulate MBL-FT exchange is more questionable (because of possible velocity gradient across the boundary and lack of mixing). In some large-scale experiments, an exchange velocity is derived from the measured exchange of ozone or water vapor; in which case we terminate the column at the top of the MBL and use the measured exchange velocity. For the case where we have only the numerically generated data, the exchange coefficients themselves define the extent of the MBL and the exchange with the FT is determined by the magnitude of these coefficients, plus any exchange that results from synoptic-scale vertical velocities generated by the mesoscale model.

The mesoscale model calculates (sub-grid) turbulent mixing by the boundary layer parameterization used in the model. Large-scale subsidence/lifting (large compared to the grid scale) are resolved by the numerical solutions to the fluid mechanical equation. The turbulent mixing coefficients describe the statistical effect of mixing due to eddies of the smallest sizes up to and including the so-called "large scale eddies" which have dimensions comparable to the height of the MBL. The characteristic length which separates the largest eddies from the large-scale vertical velocities generated by the model is, of course, not well defined. But the same division of the two mechanisms, which results from the mesoscale model treatment, is used in the aerosol calculations.

In the original aerosol model (Fitzgerald et al., 1998a, 1998b; Gelbard et al., 1998) large-scale vertical motions were not included. Locally, the effects of turbulent mixing in the MBL are much stronger than large-scale divergence which can often be neglected. Over longer periods of time and for exchange with the free troposphere, the large-scale vertical motions would appear to be important. If, for no other reason, inclusion of large-scale vertical velocities is necessary to evaluate just how important vertical velocities are relative to turbulent mixing and when, if ever, the large scale motions can be ignored. Availability of the output of the mesoscale model gives a set of vertical velocities and mixing coefficients that should be consistent and realistic. The possible importance of vertical velocity is suggested by the observations (J.S. Reid, private communication), which found sea-salt aerosol in the outflow regions from tropical disturbances. Whether or not the updrafts that are responsible for these events are on a large enough horizontal scale to be captured by the model has yet to be evaluated.

This report describes how vertical motions are included in the current 1-D aerosol model. The task of including vertical velocities was more difficult than originally anticipated, largely because the amount of mass added or subtracted to a vertical cell (due to horizontal convergence/divergence) must exactly balance the difference in that which flows through the upper and lower cell boundaries for each size section in the case when there is no vertical

gradient in the mass densities of the sections. *The condition that there be no change in the mass in a vertical cell when there was no vertical mass gradient for all convergent/divergent cases of air flow is the primary test for judging whether or not the algorithm is correct.* Any imbalance gives a spurious source/sink of particles that can causes a large excess/deficit of aerosol mass with time. Of course, if there is any gradient in the mass density, that gradient must be moved up/down depending on the vertical velocity.

II. ADDITION OF VERTICAL VELOCITY TO A ONE-DIMENSIONAL MODEL

A. Basic Scheme

Aerosol mass in each size section is conserved during displacements resulting from air motion and gravitational settling. If the aerosol mass density of particles in size section, i, is m_i, then conservation of mass requires

$$\frac{\partial m_i}{\partial t} + \nabla \bullet (m_i \vec{v}_i) = 0 \qquad (1)$$

where $\vec{v}_i$ is the sum of the fluid $\vec{v}^f$ and settling velocity $\vec{w}_i^g$

$$\vec{v}_i = \vec{v}^f + \vec{w}_i^g \qquad (2)$$

We will now drop the size index, i, with the understanding that the mass in each size section is conserved individually during displacements. Integration of Eq. (1) over a vertical column of volume V with base of area A gives the change of the total mass M in the column

$$\frac{\partial M}{\partial t} = -\int_V \nabla \bullet (m_i \vec{v}) dV = -\oint m\vec{v} \bullet d\vec{S} \qquad (3)$$

If the column spans one vertical cell then M becomes the mass of one size section in that cell and Eq. (3) becomes

$$\frac{\partial M_{cell}}{\partial t} = -w_t m_t A + w_b m_b A - \oint_{hor} m\vec{v}^f \bullet d\vec{S} \qquad (4)$$

where w_t and w_b are the vertical velocity components at the top and bottom of the cell and consist of both a fluid and gravitational settling component, the latter is different for each size section; i.e.,

$w_i = w^f + w_i^g$ (where i here refers to size section i).

The horizontal surface integral (Eq. (4)) represents the amount of mass that enters the cell through the sides of the column. For a 1-D model, m is the same at all points around the periphery of the column so that Eq. (4) can be written as

$$\frac{\partial M_{cell}}{\partial t} = -w_t m_t A + w_b m_b A - \langle m \rangle \oint_{hor} \vec{v}^f \bullet d\vec{S} \tag{5}$$

Where $\langle m \rangle$ is the vertically averaged mass density for the section.

The above conceptual picture cannot be precisely correct for a truly 1-D model. In a 1-D model there can be no flow into the sides of the column, and neither can there be a divergence in the horizontal velocity; i.e., w_t cannot be different than w_b. To those who object to the above conceptual picture they should view, what is called, the horizontal surface integral in Eq. (5) as a source term that must be added to the 1-D layer to balance any divergence in the vertical velocity, imposed externally on the layer. In practice we will impose a vertical velocity gradient calculated by the 3-D meteorological model at the location of the column. This source term compensates for the convergence/divergence in the fluid flow by bringing in particles from the same layer (in a manner which consistent with the 1-D hypothesis).

Mass conservation for an incompressible fluid is given by

$$\nabla \bullet \vec{v}^f = 0 \tag{6}$$

Integrating Eq. (6) over the volume of the column (within a cell) as done above for aerosol mass yields

$$-w_t A + w_b A - \oint_{hor} \vec{v}^f \bullet d\vec{S} = 0 \tag{7}$$

Equations (7) and (5) can be combine to eliminate all references to the horizontal flow and area of the side of the column

$$\frac{1}{A}\frac{\partial M_{cell}}{\partial t} = -\left[(w_t^f + w_t^g)m_t - (w_b^f + w_b^g)m_b\right] + \langle m \rangle (w_t^f - w_b^f) \tag{8}$$

This equation satisfies the necessary condition that if there is no gradient in the mass, $m_t = m_b = \langle m \rangle$, then there is no change in the mass in the cell, even if there is a divergence in the vertical velocity; provided of course, that the settling velocity is the same across the cell $w_t^g = w_b^g$. This latter condition will hold only in the case that the RH is constant with height. If one objects to the mixture of 1-D and 3-D models used in the above derivation, Eq. (8) can be justified alone on the bases of the following necessary condition: in the 1-D model there can be no change in the

mass in the cell if there is no gradient in the mass density even if there is a gradient in the vertical velocity (in the case of no RH gradients and incompressible flow).

The above scheme is implemented numerically by assigning a fluid velocity to cell, n, and testing the net velocity $(w_n^f + w_{n,i}^g)$, for a given section denoted by i. Since the velocity changes across the vertical cell, and can even change signs within the cell, assigning a single velocity to a cell introduces certain (finite difference) errors which can be severe if they are not handled correctly in the logical structure of the program. Some of these complications will be alluded to later. For net upward flow in the n^{th} cell and both adjacent cells, the change in mass of the n^{th} cell is

$$\frac{1}{A}\frac{\partial M_n}{\partial t} = -\left[(w_n^f + w_n^g)m_n - (w_{n-1}^f + w_{n-1}^g)m_{n-1}\right] + m_n(w_n^f - w_{n-1}^f) \tag{10}$$

Likewise for downward motion in adjacent cells

$$\frac{1}{A}\frac{\partial M_n}{\partial t} = -\left[(w_n^f + w_n^g)m_n - (w_{n+1}^f + w_{n+1}^g)m_{n+1}\right] + m_n(w_n^f - w_{n+1}^f) \tag{11}$$

The logic is actually more complicated because adjacent cells can have velocities in different direction so that there are four cases when the net velocity is up in cell n and four cases when the net velocity is down in cell n, giving a total of eight cases (See Figure 1). For the first terms of the above two equations, this logic is obvious and straight forward, since it is a matter of looking at the net flow cell by cell and removing the correct amount of mass and adding it to the correct adjacent cell. It is less obvious but crucial that the second term is calculated such that the airflow into or out of the given cell is consistent with the boundaries across which we move the particles using the net particle velocity. If this is not done properly, a small imbalance can act as an erroneous, and potentially, large source (or sink) of mass that accumulates with time. Figure 1 illustrates how the net fluid flow (expression in parenthesis in the last term) is calculated for the eight cases. Since the settling velocity is a function of size, this procedure is done separately for each section. For gases only the air velocities are required, i.e., $w^g = 0$. For particles the net velocity, air velocity plus gravitational settling, determines the direction and boundary which must be considered, e.g., one section may be moving up and another downward.

We have assumed here that the atmosphere is an incompressible fluid; i.e., no density variations. Appendix A shows that the vertical gradient of density in the atmosphere can be taken into account. The interpretation of the results, and hence testing of the algorithms to verify the accuracy of the algorithms, is more complicated for the compressible case. Therefore we have here assumed that the atmosphere is an incompressible fluid.

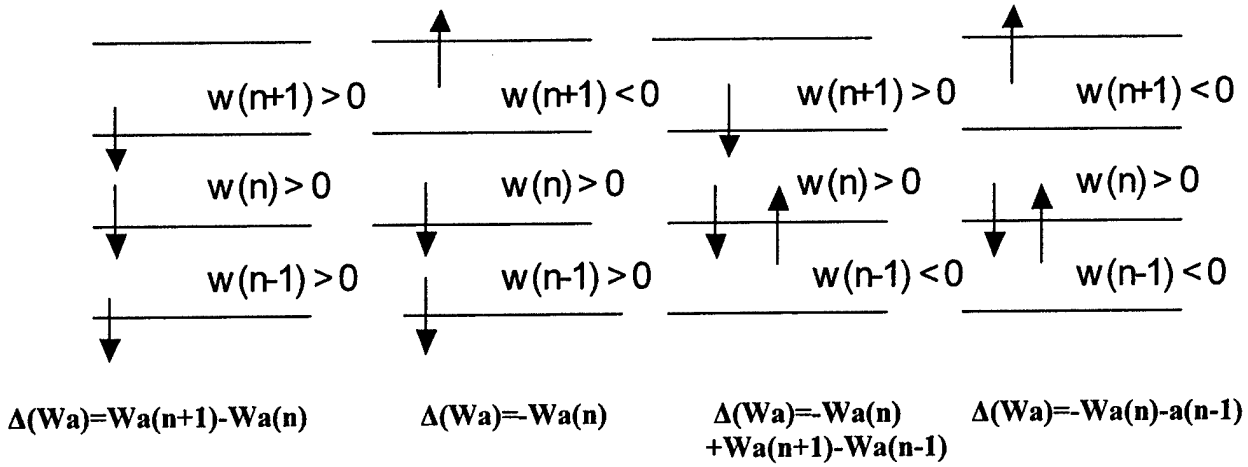

Figure 1. If w is the net vertical velocity including both gravitational lettling and vertical air velocity and Wa is the air velocity, then the added air (velocity) consistent with the vertical motion of the particle in the given cell and section is given by **Δ(Wa).** For downward motion of the particle in cell n, **Δ(Wa)** is the appropriate airflow into or out of the cell n for a given section, where positive flow is downward. There is a similar diagram when the flow in cell n is upward.

B. Aerosol flux in terms of density functions.

In the analysis above leading to Eq. (8), the particles in a section are assumed to be monodisperse whereas in the model the fluxes, such as $(w_n^f + w_n^g)m_n$, are calculated from density functions across both the size sections and vertical cells. In the model the size distribution is represented by discrete size sections of finite width. To increase the accuracy of the model the mass concentration within a single section is represented by a density function

$$\mu(\upsilon) = \alpha\upsilon^{\sigma} \tag{12}$$

Where υ is the mass (or volume) of the particle and where the slope σ is chosen such that the number concentration of particles is preserved for number preserving aerosol processes (Gelbard et al., 1998). Integration of the density function across the section i is, by definition, the mass density m, so that

$$\alpha_i = \frac{(\sigma+1)m_i}{\upsilon_{i+1}^{\sigma+1} - \upsilon_i^{\sigma+1}} \qquad \text{when } \sigma \neq -1$$

$$\alpha_i = \frac{m_i}{\ln(\frac{\upsilon_{i+1}}{\upsilon_i})} \qquad \text{when } \sigma = -1$$

Where υ_i and υ_{i+1} are the lower and upper boundaries of the section.

In addition to the density function across the sections, there is also a weighting function which varies linearly across the cell with the slope, *a*, determined by the concentration in adjacent cells. This weighting factor is given by $(1+az)$ where $z=0$ is the center of the cell. See Gelbard et al. (1998) for a description and improved accuracy achieved by using these density functions. The earlier analysis includes only the effects of the gravitational settling velocity. Here we extend the analysis to include upward or downward fluid motion in addition to gravitational settling. We follow the notation of the prior paper in writing the Stokes fall velocity as

$$w^g(\upsilon)=c\upsilon^{\frac{2}{3}} \qquad \text{where} \qquad c=\frac{\rho^{\frac{1}{3}}g}{18\eta\left(\frac{\pi}{6}\right)^{\frac{2}{3}}} \tag{13}$$

and where ρ, g, and η are the density of the particle, gravitational constant and kinematic viscosity of air, respectfully[1]. The mass removed from the cell during a downward shift is equal to the mass removed between the bottom of the cell $\left(-\Delta z/2\right)$ and the distance $(shift - \Delta z/2)$ where Δz is the width of the cell in question. The change in mass density resulting from loss out the bottom of the cell is

$$\Delta m=\left(\frac{\Delta M}{\Delta z}\right)=\left(\frac{1}{\Delta z}\right)\int_{\upsilon_i}^{\upsilon_{i+1}}\alpha\int_{\frac{\Delta z}{2}}^{shift-\frac{\Delta z}{2}}\upsilon^{\sigma}(1+az)dz\,d\upsilon \tag{14}$$

Where shift is the vertical shift (as a function of size) which results from settling and downward air movement

$$shift=\left(w^f+c\upsilon^{\frac{2}{3}}\right)\Delta t \tag{15}$$

Where Δt is the time step. Integration of Eq. (14) yields

$$\frac{\Delta m\,\Delta z}{\Delta t}=m\left\{w^f\left[1-\frac{a}{2}\left(\Delta z-w^f\Delta t\right)\right]\right\}+\alpha c\left\{\left[1-\frac{a}{2}\left(\Delta z-2w^f\Delta t\right)\right]\left(\frac{\upsilon_{i+1}^{\sigma+\frac{5}{3}}-\upsilon_{i+1}^{\sigma+\frac{5}{3}}}{\sigma+\frac{5}{3}}\right)+\frac{ca\Delta t}{2}\left(\frac{\upsilon_{i+1}^{\sigma+\frac{7}{3}}-\upsilon_{i+1}^{\sigma+\frac{7}{3}}}{\sigma+\frac{7}{3}}\right)\right\} \tag{16}$$

[1] The slip correction factor has been neglected. The settling velocity for particles, which are small enough for the slip correction to be important, is entirely negligible compared to atmospheric motions (turbulent diffusion and vertical air velocities).

If $w^f = 0$, Eq. (20) in Gelbard et al. (1998) is obtained. If there is no gravitational settling, $c=0$ and only the first term survives; furthermore, if a is also zero, there is no vertical gradient in the mass concentration and the flux out of the cell is given by $m\,w^f$ as expected.

For a net upward displacement, i.e. for those sections where the upward air velocity exceeds the gravitational settling, the limits on the z-integration in Eq. (14) is from

$$\left(\frac{\Delta z}{2} - |shift|\right) \text{ to } \frac{\Delta z}{2}$$

and the integration results in the following equation:

$$\frac{\Delta m\,\Delta z}{\Delta t} = m\left\{w^f\left[1+\frac{a}{2}\left(\Delta z - |w^f|\Delta t\right)\right]\right\} - \alpha c\left\{\left[1+\frac{a}{2}\left(\Delta z - 2|w^f|\Delta t\right)\right]\left(\frac{\upsilon_{i+1}^{\sigma+\frac{5}{3}} - \upsilon_{i+1}^{\sigma+\frac{5}{3}}}{\sigma+\frac{5}{3}}\right) + \frac{ca\Delta t}{2}\left(\frac{\upsilon_{i+1}^{\sigma+\frac{7}{3}} - \upsilon_{i+1}^{\sigma+\frac{7}{3}}}{\sigma+\frac{7}{3}}\right)\right\} \tag{17}$$

In keeping with the notation in the original paper, a downward displacement is positive and an upward velocity is negative in Equations (16) and (17). Equation (17) can be obtained from (16) by (i) changing the sign on a and c and (ii) taking the absolute value of w^f.

Equations (16) and (17) replace the $(w_n^f + w_n^g)m_n$ terms in Equations with (10) and (11) where it should be noted that

$$\Delta M_{cell} = (A\,\Delta z)\Delta m = \Delta z \Delta m \tag{18}$$

Without loss of generality we can set A=1 m^2; i.e., a column of unit cross-sectional area. If we keep the dimensions of A we get aerosol mass density in units of mass per unit volume. In a truly 1-D situation the mass density has units of mass per unit length, in which case A does not enter.

In the case of a monodisperse aerosol, or for sections of infinitesimal width, conservation of number of particles follows directly from conservation of mass, i.e., the set of equations for number density is the same as for mass density and related by a single particle mass $\overline{m_i^p}$ for section i

$$N_i = \frac{m_i}{\overline{m_i^p}} \tag{19}$$

For the case where the mass density is allowed to change across the section, (as in Eq. [12]), the number of particles are not generally conserved. In Gelbard et al. (1998), the rigorous method to assure conservation of number as well as mass is presented for the case of gravitational settling (no air motion). However in implementing particle conservation in the code, particle

conservation was calculated using the approximation that a particle which settles out of a cell has a mass equal to the mean particle mass of the layer it is leaving. At the end of the time step, a new mean particle mass $\overline{m_n^p(new)}$, for a given section, was calculated from

$$\overline{m_n^p(new)} = \frac{M_n^{orig} - \Delta M_n^{out} + \Delta M_{n+1}^{in}}{\frac{M_n^{orig} - \Delta M_n^{out}}{\overline{m_n^p(old)}} + \frac{\Delta M_{n+1}^{in}}{\overline{m_{n+1}^p(old)}}} \tag{20}$$

where M_n^{orig} is the mass in the section at the start of the time step and the numerator is the mass in cell n at the end of the time step. The denominator is the number of particles in the cell at the end of the time step, $\overline{m^p(old)}$ is the mean particle mass, in the subscripted cell, at the beginning of the time step. The section index, i, has been dropped since all quantities are for the same (dry) section.

In the new version of the code that includes vertical air motion, we have retained the approximation that particles removed from a cell have the same mean particle mass (for a given cell) as the layer from which it is removed. Conservation of number is now maintained by calculating the new particle mass for a given section from

$$\overline{m_n^p(new)} = \frac{M_n^{orig} - \Delta M_n^{out} + \Delta M_{n\pm1}^{in} \pm \Delta M_n^{horz}}{\frac{M_n^{orig} - \Delta M_n^{out} \pm \Delta M_n^{horz}}{\overline{m_n^p(old)}} + \frac{\Delta M_{n\pm1}^{in}}{\overline{m_{n\pm1}^p(old)}}} \tag{21}$$

where ΔM_n^{out} and $\Delta M_{n\pm1}^{in}$ are the amounts of mass moved (up or down) out of cell n and into the cell n from adjacent cells, respectively. The direction of movement is determined by the sum of the settling velocity and the vertical air velocity. ΔM_n^{horz} is the mass added to cell n as determined from the divergence of the vertical velocity field. Equation (20) is somewhat schematic and must be modified when the vertical velocity goes to, or through, zero in a given cell.

C. Implementation.

Calculations of organized vertical motions are carried out in the subroutine "MOVEIT" (turbulent mixing is done elsewhere in the code). The net vertical velocity (settling plus air velocity) for a given section and cell is calculated and, depending on the direction of the net velocity, Eq. (16) or (17) is used to calculate the mass removed ($\Delta m \Delta z \Delta t$) and the mass remaining in the cell during a time step Δt. These masses are added into the appropriate cell (and section) of a temporary mass array. The mass that must be added/subtracted to each cell (and section) as a result of convergence/divergence of the fluid field is calculated from the last terms of Eqs. (10) and (11). At the end of each time step (i.e., each call to subroutine MOVEIT) the temporary mass array is used to re-set the primary mass array and to recalculate the mean particle mass in each section such that number density is also conserved.

For trace gases the procedure is much easier because there is no settling, and there are no size sections. There is however a density function across the cells so that the mass flux is just the first term of Eqs. (16) and (17) with in-flow given by the last terms of Eqs. (10) and (11), which accounts for convergence/divergence.

During testing it was found that a spurious particle source occurred at the surface and when the velocity crossed zero. The source of this error can be seen by writing Eq. (10), for upward net motion for the first cell

$$\frac{1}{A}\frac{\partial M_1}{\partial t} = -\left[(w_1^f + w_1^g)m_1\right] + m_1 w_1^f \qquad (22)$$

Where the terms for the cell below the surface have been omitted since nothing can move up out of the earth's surface. In the term that accounts for convergence there is no longer a gravitational term to balance the gravitational settling term in the cell, as there is in all other cells. This has the same effect as introducing a large (settling) velocity divergence at the surface (which of course is not realistic). This can be remedied by adding a gravitational flux term obtained from Eq. (17) by setting w^f equal to zero in Eq. (17). This exactly balances the upward flow out of the first cell with the inflow; when there is no gradient in mass.

To facilitate one who is interested in understanding the code, we here provide definitions of several key variables used in the subroutine MOVEIT:

IFLIP is an integer that equals 1 or –1 depending on whether the particles in a given section and cell are moving down or up, respectively.
NNOS is an offset index that is 0/2 for downward/upward displacement.
TERM is the mass removed from the current section L and cell N.
HTERM is the mass added/subtracted (horizontally) due to divergence of the vertical velocity.
TERM00 is the correction when the velocity goes through zero in the current cell.
TRANQ(K,L,N) is the temporary array for the mass of component k in section L and cell N, where the array is offset one cell (N+1) from that of the primary array Q(k,l,n), such that the mass remaining in the cell after the time step is placed in TRANQ(K,L,N+1), the mass moved down goes in N and the mass moved up goes in N+2.
TRANN(L,N) is an array which holds the mass removed vertically from cell N and is used in calculating the mean particle mass.
VMEANT(L,N) is a temporary array for VMEAN, so that VMEAN(L,N) will not be overwritten when moving particles upward.
Analogous variables have been introduced for the gas calculations: TRANQG(N), HTERMG and FMOVE, the later being the mass of gas removed from a cell.
In the program the sign convention for the velocity is positive for downward velocity and negative for upward velocity: and opposite to that used in the preceding equations.
Other definitions remain unchanged:
Q(K,L,N) is mass of component K in section L and cell N.
QT(L,N) is the mass of all components in section L and cell N.

(The indexing in the program is actually not that indicated above (K,L,N) but rather a continuous string: [K+KCOMP*(L-1)+M*KCOMP*(N-1)], where KCOMP and M are the number of components and the number of sections, respectively.)

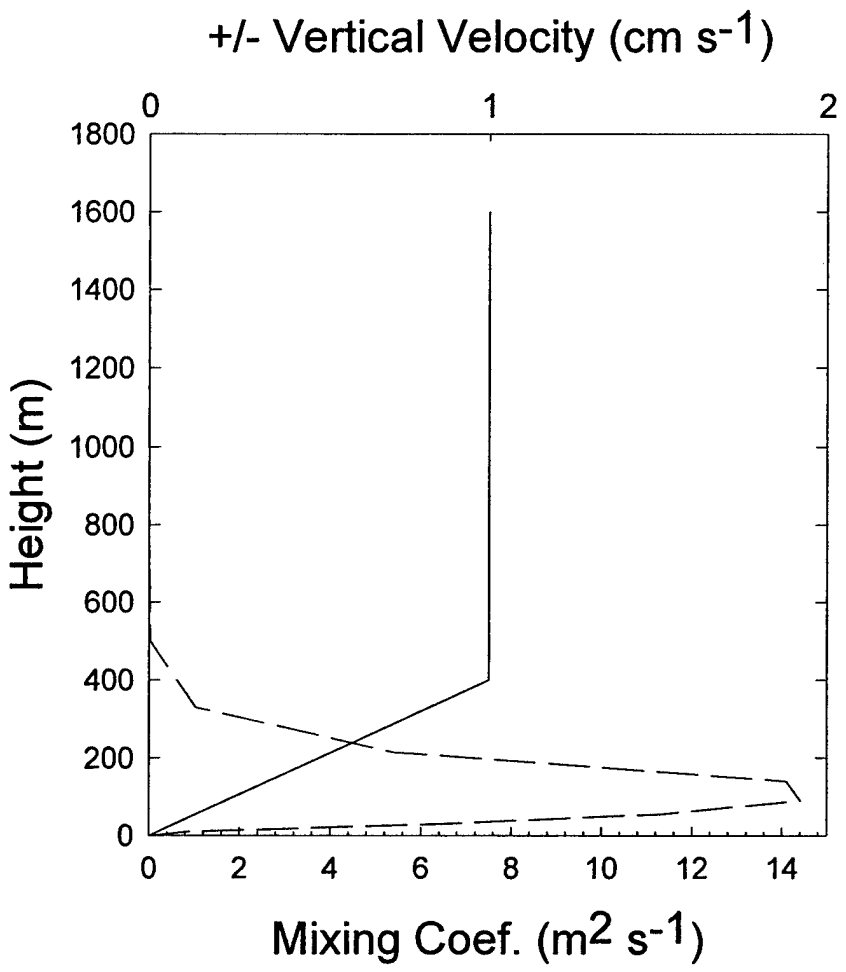

Figure 2. Vertical velocity profile (solid line) used in solutions shown in Figures 3-27 and the profile of the turbulent mixing coefficient introduced when mixing is included in the solutions

III. TESTING OF THE MODEL

A. Testing of the effect of vertical velocity in isolation.

Many tests of the effect of vertical velocity on the size distribution with all other aerosol processes turned off were executed. These included: (1) exponentially increasing vertical velocity with height to some height, H, above which the velocity remains constant. Both upward and downward fluid velocities were tested. (2) Linearly increasing upward vertical velocity (convergence) to some height, h, at which point the velocity linearly decreased (divergence), crossed through zero and became downward, and at some greater height, H, the vertical velocity

becomes constant in the downward direction. The reverse of this case where the linearly increasing velocity is downward near the surface was also checked. (3) Constant upward and downward vertical velocity (no convergence/divergence) were tested. In this case the program had to be modified so that the vertical air velocity was not zero at the surface as required by the program. Here we will show results only for the case (4) where the vertical velocity increases linearly with height, H, after which it remains constant with height. The results will be shown for both upward and downward air velocities for the velocity profile shown in Figure 2 by the solid line. For cases (1) - (3), tests were limited only to the effects of vertical velocity. Many more cases, including the interaction with other processes were done for case (4) some of which are shown below. For the cases shown in Figures 3-11, turbulent diffusion is turned off and any "diffusion" observed is a result of numerical diffusion. In later cases where turbulent diffusion is included, it will be seen to totally dominate any numerical diffusion which is introduced by the numerical methods.

In all these tests, it is useful to initialize the model with a size distribution that is the same at all altitudes below some given height and then changes abruptly to a different constant size distribution above that height. The region of constant mass with height gives a region in which no change in concentration should be observed even if there is convergence/divergence in the vertical air velocity because there is no gradient in concentration. The 'horizontal' in/out flow should just balance the difference between the masses flowing out the top and in the bottom of a cell (or visa versa). The rate of change in the height where the abrupt change occurs should agree with that predicted by the vertical velocity. For gases the motion follows the air velocity and the results are easier to interpret than for particles, the larger of which, may have fall velocities that are comparable to, or greater than, the air velocity.

Downward vertical velocity. The solution for a downward vertical velocity profile as shown in Figure 2 is given in Figures 3-7. All process are turned off except equilibration with the ambient RH, which is taken to be constant at all heights at a value of 70% RH. This insures that the settling velocity of a given particle remains constant with height. The basic time step is 30 seconds and data output every 8 hours. Above 400 m the velocity is downward at 1 cm s^{-1} (no divergence). Below 400 m the vertical velocity decreases linearly to zero, which requires horizontal divergence. The vertical domain of the model extends to 1550 m (top cell extends from 1500 to 1550 m), and for the case shown no material enters the domain from the top. The thickness of the vertical cells were set at 20 m below 200 m and 50 m between 200 m and 1550 meters. Figure 3 shows the evolution of the concentration profile for a trace gas (scalar contaminant) which has no gravitational settling velocity. The solid line shows the initial profile of SO_2. Above 400 m where the velocity is constant, the step function that occurs initially in the cell bounded by 600 and 650 m and the discontinuity at the top, caused by no new material entering the domain, moves downward at a constant velocity of 1 cm s^{-1}. The discontinuity broadens vertically as a result of numerical diffusion. It is important to notice that the profiles below the discontinuities (and the diffusion broadening) remain constant with height - even below 400 m where there is air flow divergence. This is a test of how well the convergence/divergence part of the algorithm is working. While Figure 3 is for a trace gas, the same behavior is obtained for particles that have negligible fall velocities (small compared to 0.1 cm s^{-1}).

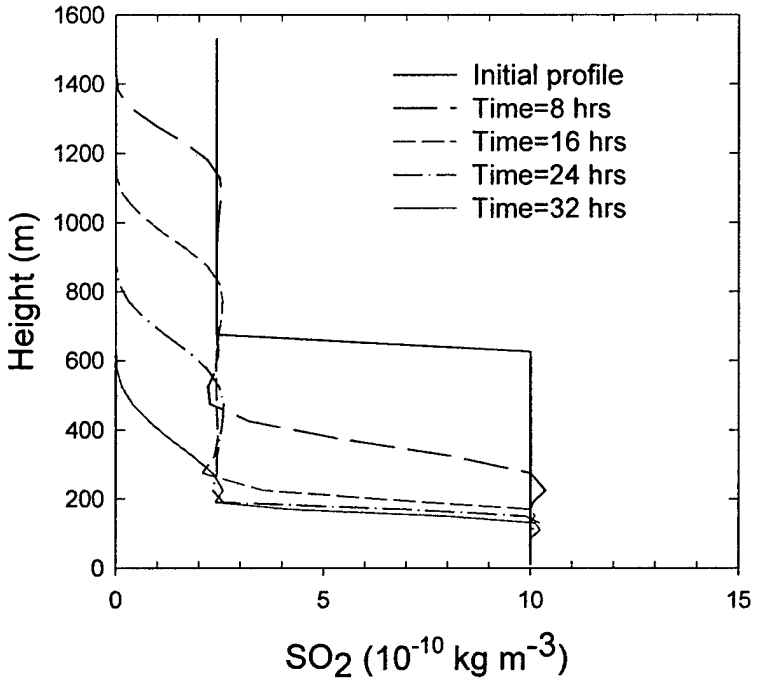

Figure 3. Change in the concentration of a trace gas for a downward vertical velocity profile shown in Figure 2. The solid line gives the initial profile.

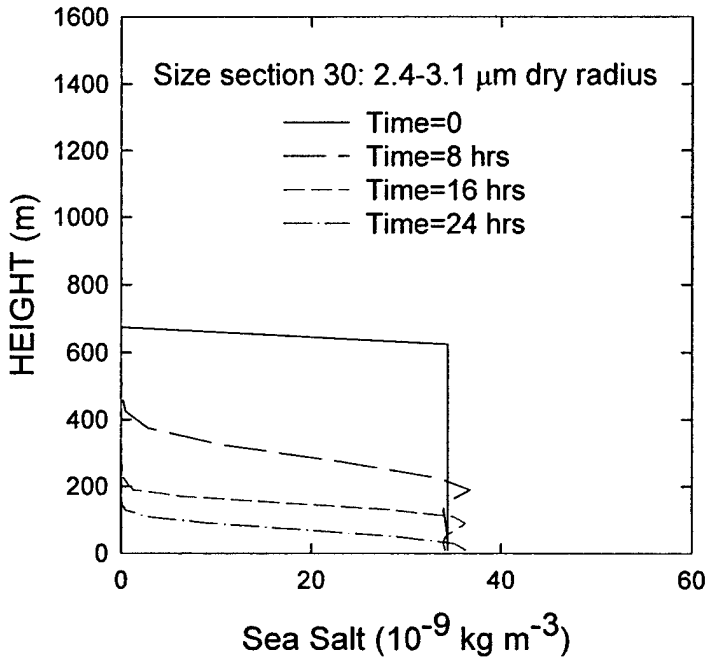

Figure 4. Downward movement of sea-salt particles of dry radius 2.4-3.2 μm. Same case as in Figure 3. Solid line is initial profile.

Figure 4 shows the downward movement of the sea-salt component of particles in the section 30 where the dry radius is 2.4-3.1 μm. In the model these are assigned to be sea salt particles and will sometimes be referred to as such. The downward movement at the lowest heights (below 200 m) is greatly enhanced over that shown in Figure 3 as a result of gravitational settling. The solid line with crosses in Figure 5 shows the initial size distribution in all cells above 650 meters. Also shown in Figure 5 are the size distributions in the cell at 1150-1200 m at 8 hrs and 16 hours. At 8 hours the size distribution remains unchanged because the cells above have the same size distribution and the depletion of particles propagating downwards from the top has not yet reached 1200 meters. After about 11 hours the concentration starts to drop precipitously since no new particles are being introduced at the top of the domain. The concentration of particles after 16 hours has dropped by two and a half orders of magnitude (it would be zero if it were not for numerical diffusion).

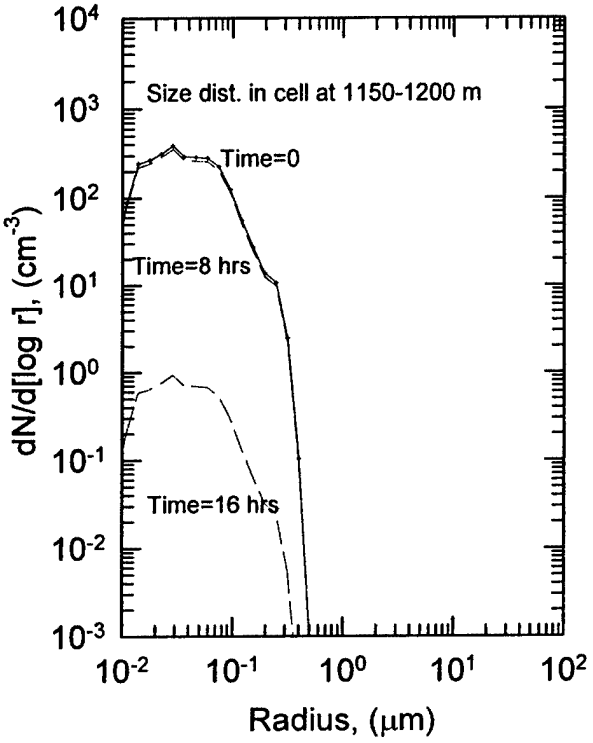

Figure 5. Change in the size distribution in the cell bounded by 1150 and 1200 meters with downward velocity profile shown in Figure 2. Solid line with crosses is the initial size distribution at all heights above 650 meters. No new particles are allowed to enter the domain, so that all particles initially above 1150 are below 1150 meters after16 hours.

The curve denoted by crosses in Figure 6 is the initial size distribution in all cells below 600 meters. The size distribution here is the result of both sulfate and sea-salt aerosol, whereas Figure 4 includes only the sea-salt component which is dominant at sizes larger than about 0.2

μm and extends initially only to 650 meters.[2] Also shown is the evolution of the size distribution in the cell bounded by 400 and 450 meter. At 16 and 24 hrs the initial size distribution has been displaced by the size distribution which initially existed above 600 meters. In fact, the displacement had mostly occurred by 8 hours (the flow displacement in 8 hours is 288 m). By 32 hours, downward movement of clean air from 1600 m had depleted the particle concentration at 400 m by a factor of four.

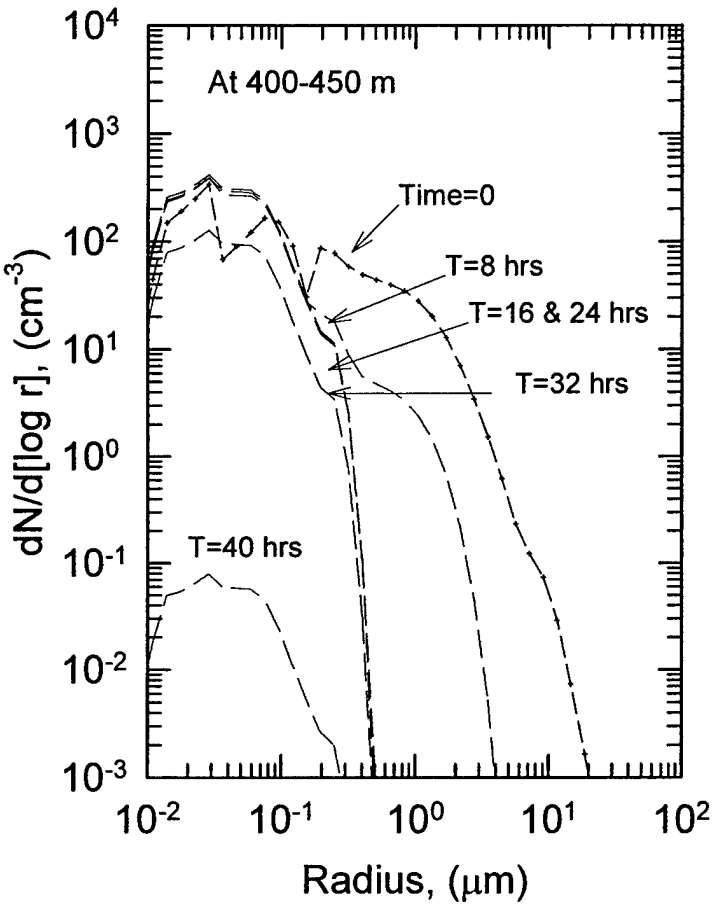

Figure 6. Evolution of the size distribution in the cell bounded by 400 and 450 meters

In the lowest cell (0-20 m) no particles are removed by vertical airflow since the vertical velocity goes to zero at the surface. The removal is by divergence and surface deposition. Figure 7 shows the evolution of the size distribution in the lowest cell. The loss of large particles is via gravitational settling. The small particles moving downward into the lowest cell under the influence of the decreasing vertical airflow are just balanced by horizontal divergence out of the cell. The fact that the small particle end of the size distribution does not change with time is validation that the divergence/convergence part of the program is working well.

[2] The designation of components as sulfate and sea-salt aerosol is of no consequence to the behavior which is being studied here. However it is the way the components are specified in the model. The aerosol is internally mixed.

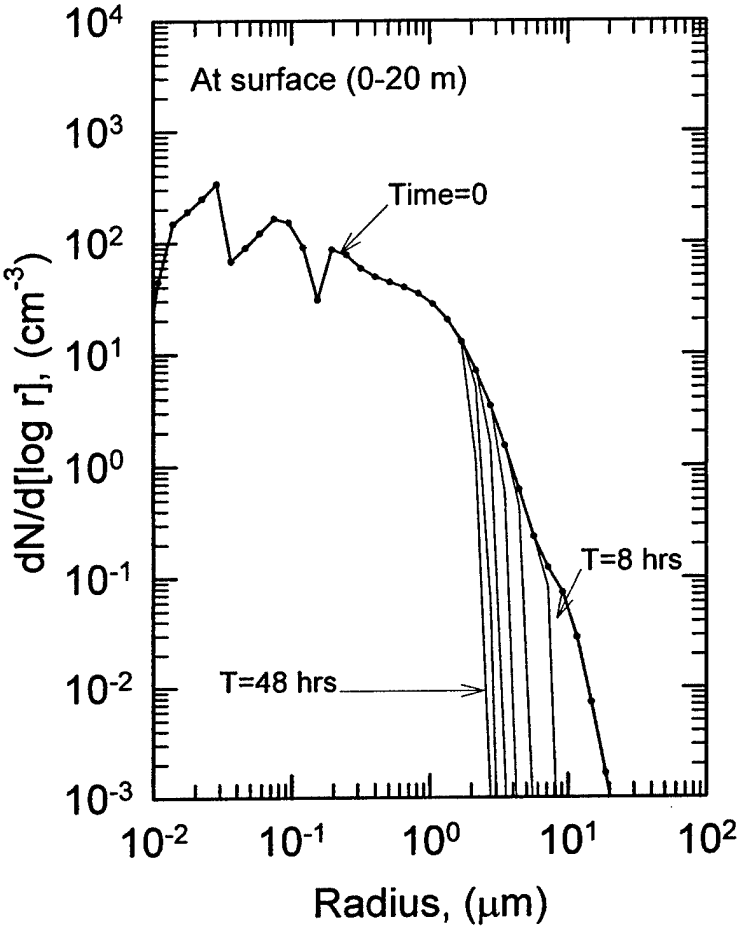

Figure 7. Evolution of the size distribution in the lowest cell (0-20m). The downward air velocity is approaching zero at the surface and particles from above are mostly removed by divergence before reaching the lowest cell. The loss of larger particles is due to gravitational settling.

Upward vertical velocity. The situation and interpretation is more complicated for upward air velocities because the net velocity of the particle can change directions depending on relative magnitudes of the air and gravitational settling velocities, and can even be in opposite directions in adjacent cells. For a vertical air velocity which increases linearly with height there will be some height at which the net velocity changes direction. The numerical solution for the case where the upward air velocity profile is given by Figure 2, are shown in Figures 8 through 11. For particles as small or smaller than those in section 25 (0.73-0.93 mm), the settling velocity is so small that they move upward even in the lowest cell (center at 10 m) as indicated in the top graph of Figure 8. The constancy of the concentration with height as the particles move upward indicates that the (horizontal) convergence into the cells below 400 meters is being properly handled. {Note: we will later set the air velocity to zero in the lowest cell and discuss the reason that it gives a more realistic result.} In section 27 (1.18-1.5 μm radius), shown in the lower graph

of Figure 8, the settling velocity in the lowest cells is greater than the upward air velocity causing nearly complete depletion of particles in the lowest cell in eight hours. Particles in cells above the lowest cells are moving upward. As the particle size increases, the reversal height moves upward, as shown in Figure 9, (because the vertical velocity is increasing with height). As the reversal altitude increases, the concentration in the lowest cell is maintained for an increasing longer time by particles moving down from above (but from below the reversal point) as is seen in Figure 9b and as will be discussed in connection Figure 10. The increased settling velocity of the larger particles also slows the upward movement as seen in the figures at altitudes above 650 meters.

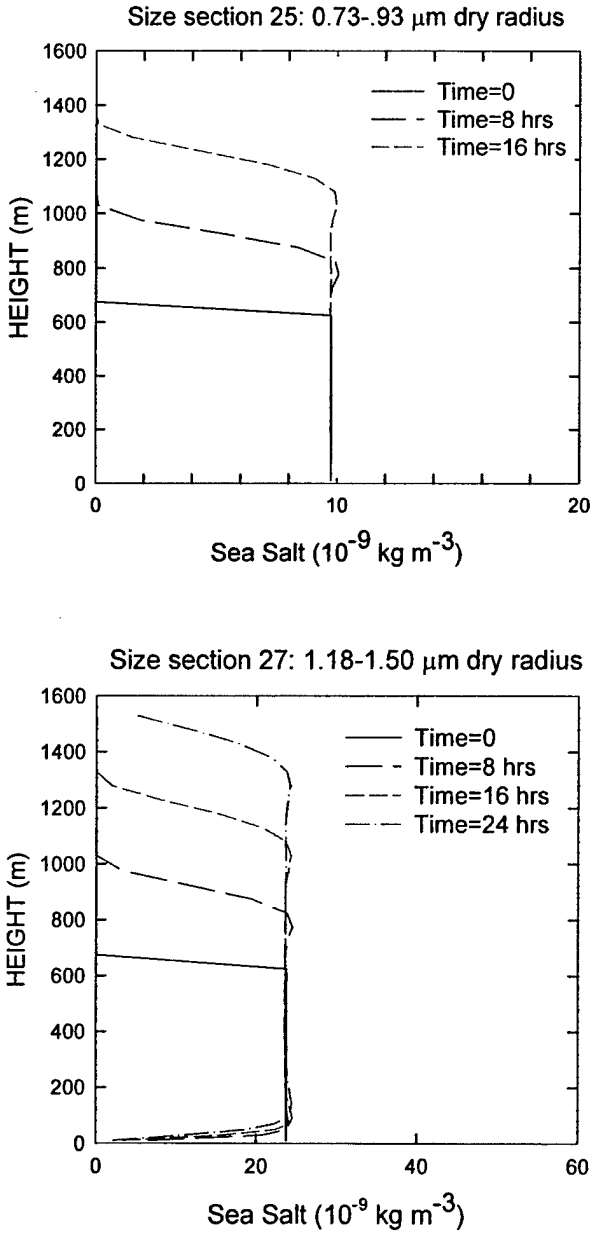

Figure 8. Sea-salt concentration in size sections 25 and 27 at 8-hour intervals. Note how constant the concentration remains in the vertical, illustrating that convergence is being handled correctly.

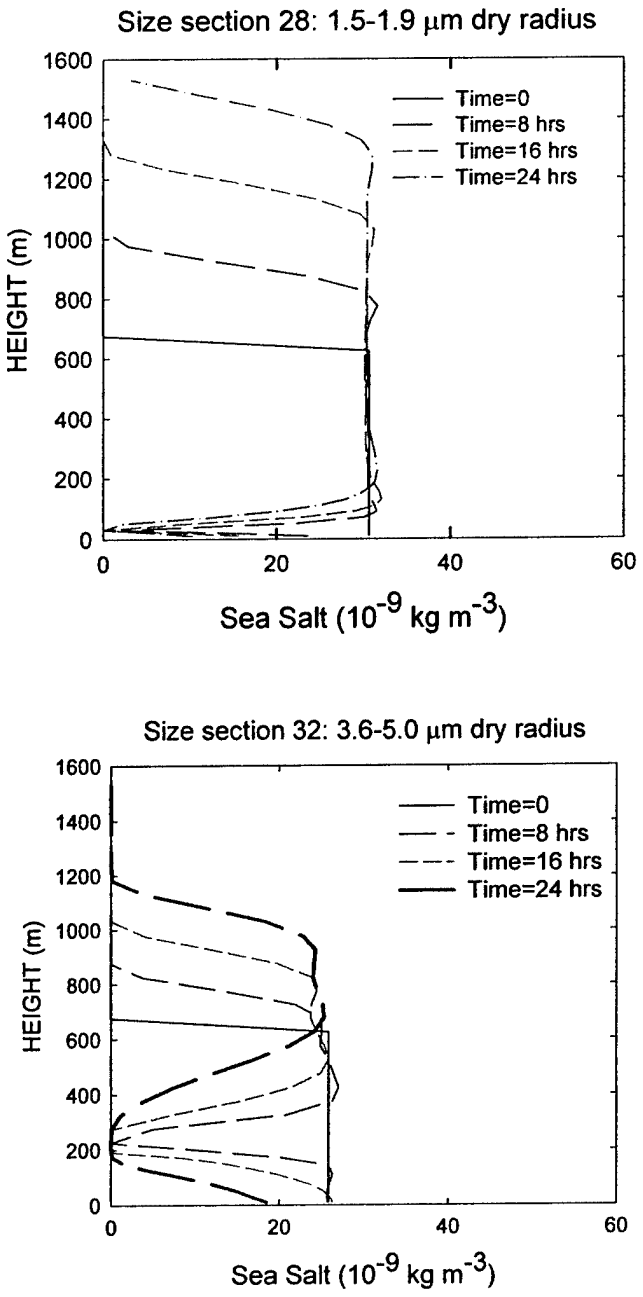

Figure 9. Sea-salt concentration in size sections 28 and 32 at 8-hour intervals, illustrating the increasing height of the reversal point as size of particle radius increases.

The change in the size distribution in the lowest cell every eight hours for 48 hours is shown in Figure 10. The maximums and minimums developing at larger sizes can be explained by the behavior shown in Figures 8 and 9. The minimum at about 1.3 μm radius is in section 27 where the low concentration results from the low reversal point; i.e., no particle are available to flow downward into the lowest cell. The maximum at 1.7 μm is in section 28 (Figure 9a) and results because the reversal point is now at a higher altitude and particles between the lowest cell and the breakpoint are settling downward into the lowest cell. At eight hours all particles in

sections with radius greater than 1.5 μm and smaller than 10 μm are the same as at time zero. Of course these sections will eventually be depleted (as shown in Figure 10) as the region between cell 1 and the reversal point is depleted. The correct, but rather strange behavior exhibited in Figure 10 is the result of the interplay between the velocity profile (Figure 2), the dependence of the settling velocity on radius, and the shape of the initial concentration and velocity profiles. At radii greater than about 5.0-6.3 μm (section 33) the gravitational settling velocity is greater than the vertical air velocity at all heights and the aerosol concentration collapses downward with time, as shown in Figure 11 for section 34.

B. Including other processes which effect the vertical distribution.

We would expect other processes, which also cause gradient transport, to interact strongly with the vertical velocity transport discussed above. Other processes that effect gradient transport are: turbulent mixing, surface deposition (and/or lower boundary condition), free troposphere exchange (and/or upper boundary condition), and a localized source of aerosols. Any localized source of aerosols will produce a gradient in concentration, but the primary one of interest here is the source of sea-salt aerosol at the ocean surface.

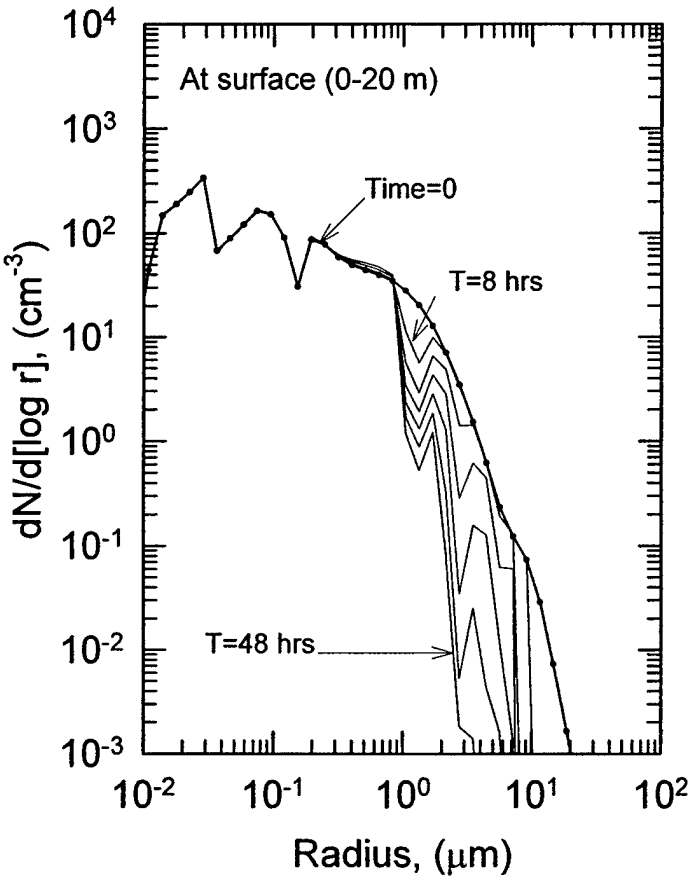

Figure 10. Size distribution in the lowest cell at 8-hour intervals

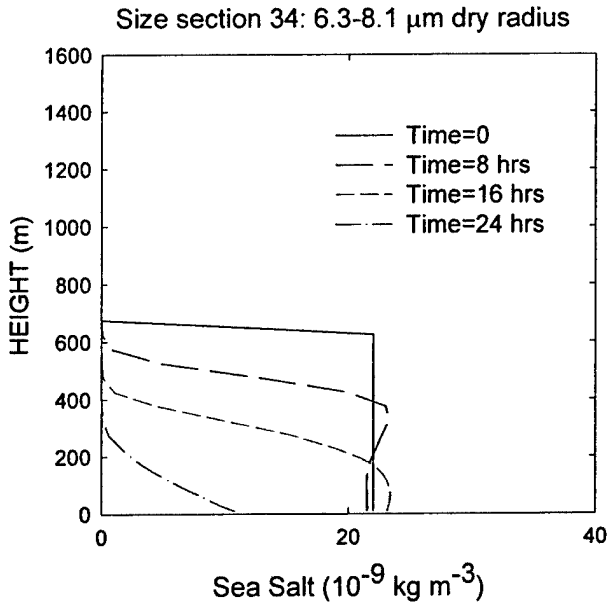

Figure 11. Sea-salt concentration in size section 34 at 8-hour intervals with upward air velocity.

Adding turbulent mixing. The vertical broadening (and overshoot) of the initial step in concentration, which occurs between 600 and 650 m in Figures 8 and 9 with increasing time, is the result of numerical diffusion. Numerical diffusion is also apparent in Figure 3 for trace gases. In a real atmospheric simulation, which includes turbulent diffusion, the degree of numerical diffusion seen in these solutions is totally obscured by real turbulent diffusion which occurs in the atmosphere boundary layer (Fitzgerald et al., 1998a)

Figures 12 to 14 show the solution when turbulent diffusion is added, where the dashed line in Figure 2 shows the profile of turbulent mixing coefficients used in these and subsequent solutions. This particular combination of profiles of turbulent mixing coefficients and aerosol concentrations is not realistic, since the drop in concentration occurs at 625 m and the mixing coefficients drop off at about 400 m. For testing the model, however, it is better not to have the two discontinuities at the same height. Figure 12 shows the evolution of the vertical concentration profile in section 32, and should be compared to Figure 9b when there is no mixing. Below 400 m the turbulence is strong and results in a nearly uniform concentration. Above 500 m the mixing drops to nearly zero and the upward air velocity transports the particles which were originally between 400 and 600 m upward as in the case when there was no turbulence. Below about 500 m the combined action of gravitational settling and turbulence transports particles downward. As the particle concentration tends to separate at the reversal point seen in Figure 9b, the turbulent mixing fills in the gap by increasing the downward flux from above and inhibiting the downward gravitational flux below the reversal point.

Figure 13 shows the case when the net (air plus gravitational velocities) is downward at all heights. Figure 13 should be compared to Figure 11 when there is no mixing. The mixing destroys the concentration gradient in the region of strong mixing (below 400 m). As the top of

the concentration gradient settles into the region of strong mixing, the turbulence acts on the gradient, opposing gravity, tending to keep the particles suspended for a longer period of time.

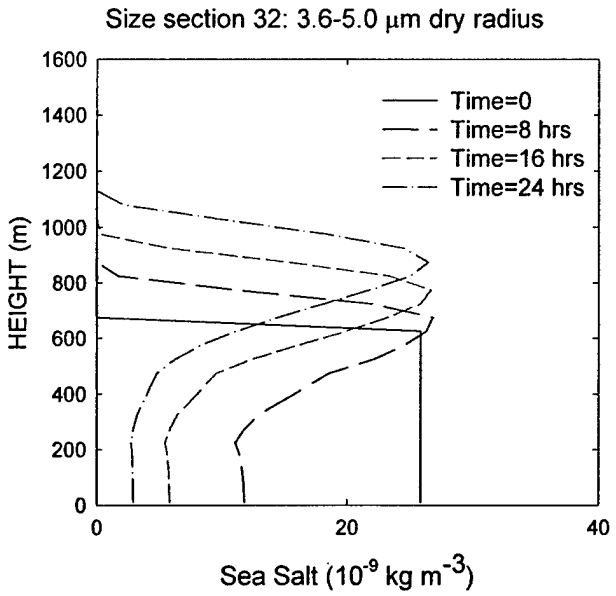

Figure 12. Size section 32 with up velocity and turbulent mixing. The turbulent mixing profile is shown in Figure 2. Figure 9b is the same section when there is no turbulent mixing.

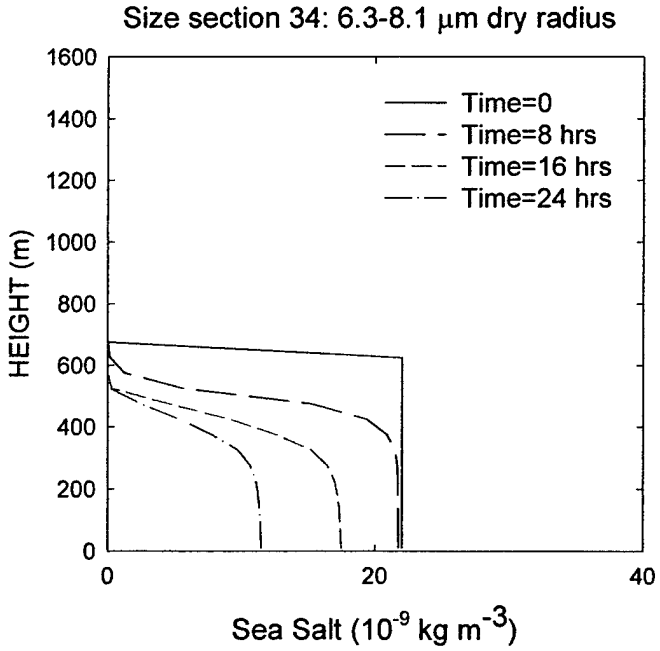

Figure 13. Size section 34 with up velocity and turbulent mixing. The turbulent mixing profile is shown in Figure 2. Figure 11 is for the same section when there is no mixing.

Figure 14 shows the net effect on the size distribution in the lowest cell over a 48-hour time period. The irregularities seen in Figure 10 are smoothed out by the turbulence as expected. The one peak that remains can be traced to those particles that are nearly suspended by the upward air motion between 400 and 600 m, above the region of mixing. This peak occurs in size section 34 which is the section shown in Figure13. These particles fall slowly into the well-mixed region sustaining the particle concentration. Air motion moves smaller particles upward and out of this region while larger particles fall quickly out of this region.

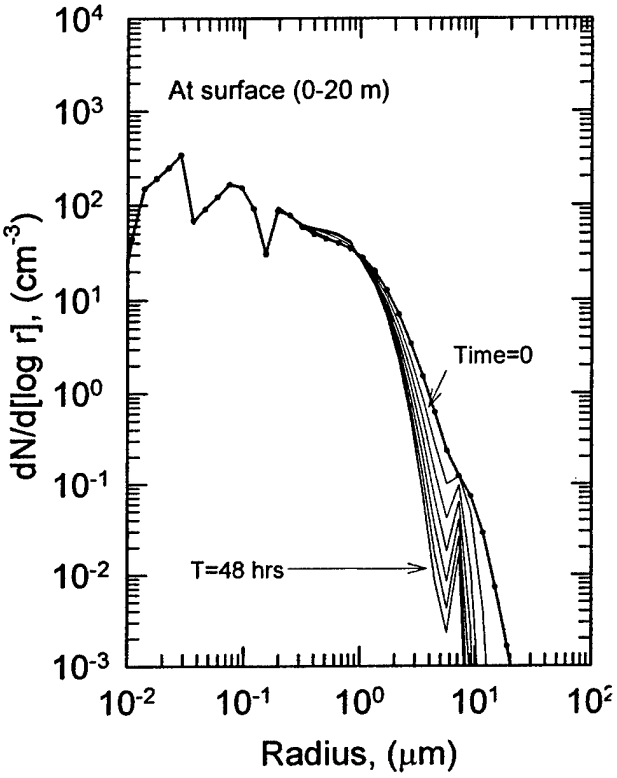

Figure 14. Size distribution at the surface with upward velocity and mixing turned on. Profiles of mixing coefficients and vertical velocities are those shown in Figure 2.

Effect of a sea-salt aerosol surface source and surface deposition. Here we turned mixing back off and turned on the surface source of sea-salt using a hybrid formulation (combination of Monahan et al., 1986 and Smith et al., 1993) given by Hoppel et al. (2002). We also extended the size range to sizes as small as 0.06 μm even though there is no justification for using the formulation below about 0.3 μm. Surface deposition was also turned on. The surface deposition was that given in Fitzgerald et al. (1998a) for all components except sea salt. For sea-salt aerosol we used only gravitational settling as shown by Hoppel et al. (2002, 2005) to be more appropriate for a surface source. The solution uses the same upward directed vertical velocity profile as before and shown in Figure 2. However, in the lowest cell the air velocity is set equal to zero instead of the value at the midpoint. The reason for this is that all particles in the cell (for a given section) move with the velocity equal to the sum of the vertical air velocity and the settling velocity. For downward air velocity, this gives a deposition velocity that can be much too large, and for upward air velocity, gives a deposition velocity that is either too small or

nonexistent if the upward velocity is greater than the settling velocity. Since the deposition velocity must indeed go to zero at the surface, setting the air velocity to zero in the lowest cell is not only reasonable but totally justifiable by the fact that turbulent mixing near the surface is much greater than that resulting from vertical velocities caused by large scale divergence. The vertical velocity in the lowest cell is now set to zero in the current version of the program.

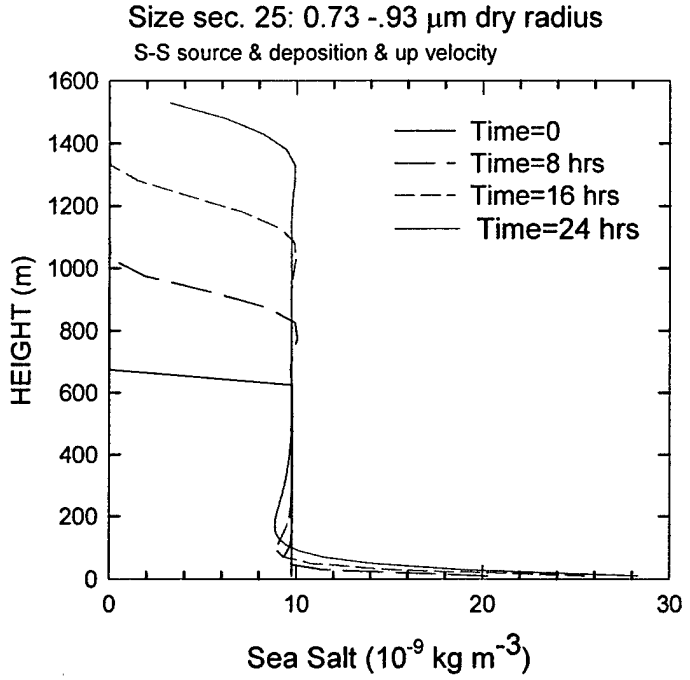

Figure 15. Vertical profiles of sea-salt concentration in size section 25 when a sea-salt source is added and there is no mixing.

The results are shown for sections 25 and 30 in Figures 15 and 16. In section 25 the net particle velocity is upward in all vertical cells (except the first where the air velocity is zero). Since there is no upward velocity in the first cell, the sea-salt aerosol is confined to the lowest cell and the concentration builds up until there is a balance between the source and surface deposition. The anomalous increasing in the concentration seen in Figure 15 in the second cell is caused by the following numerical situation: As stated earlier, the concentration distribution vertically across the cell is assumed to be linear with slope determined by the concentrations in the adjacent cells. The unrealistic large build up in the first cell gives a very large slope in the second cell. Too few particles are therefore transported upward out of the cell for the number moved into the cell as calculated from the velocity divergence using the midpoint concentration. This results in a net increase in the concentration in the cell when it should have been zero. This is an unrealistic case. When turbulence mixing is present the gradient is small and nearly linear. The minimum just above the sea-salt aerosol layer is a result of numerical diffusion that is particularly pronounced because of the very strong gradient at the surface.

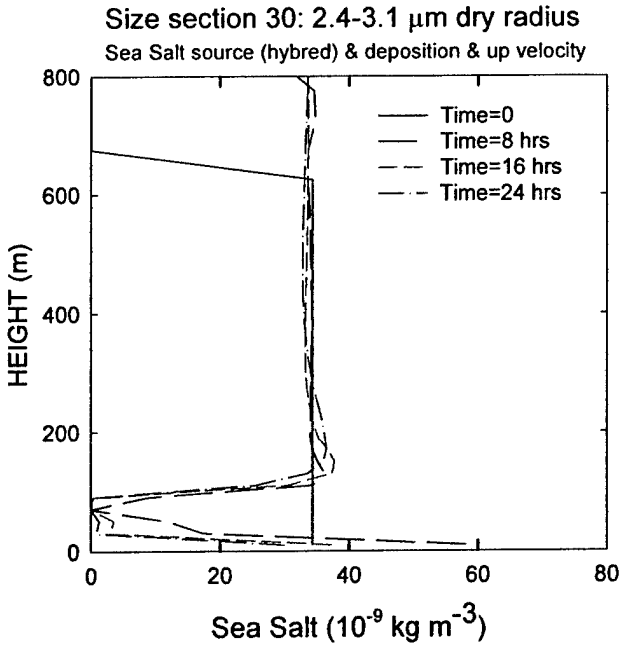

Figure 16. Vertical profiles of sea-salt concentration in size section 30 when the sea-salt source is added.

In Figure 16, size section 30, we again see the minimum caused by the reversal in the net velocity just below the 100 m height as in Figure 9b. The concentration in the first cell is limited by fallout and is therefore depends strongly on the particle radius as well as the source strength. Figure 17 shows the change in the size distribution over the first 48 hours in the lowest cell. The decrease seen at the smallest radii is caused by surface deposition. There is no sea-salt aerosol source below about 0.06 μm radius. No particle lost due to the divergence in velocity because the divergence in vertical velocity is just matched by the convergence of horizontal velocity. In the region between 0.06 and 0.5 μm there is a steady increase over the 48 hour period because the deposition is so slow that equilibrium (between surface source and fall out) is not achieved in 48 hours. From about 0.5 to 10 μm equilibrium between the source and deposition is achieved in 48 hours. The increasing time to achieve equilibrium at the largest radii is the result of particles settling into the lowest cell from above.

Add turbulent mixing. Figures 18-20 show the change that results when turbulent mixing is include where the profile of turbulent mixing coefficients is given in Figure 2 and extends to about 500 meters. Comparing Figure 18 to 15, we see that the particles injected at the surface are spread rather uniformly over the lowest 400 m and reach an altitude where the upward air velocity can transport them to higher altitudes. In Figure 18 we have also shown the 48-hour solution. Even after 48 hours the concentration is far from the steady-state value (between upward gradient mixing and gravitational fallout). The time to reach equilibrium is inversely proportional to the fall velocity and for small particles equilibrium is never reached in the atmosphere (Hoppel, 2002).

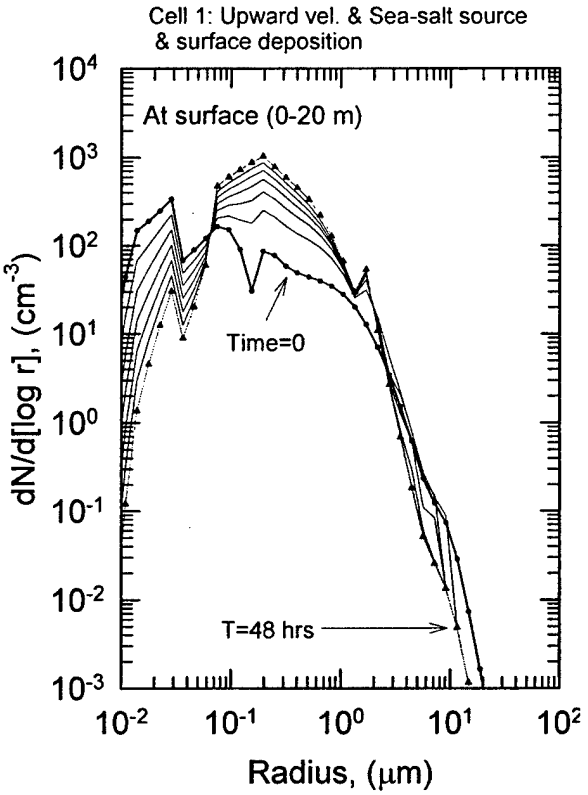

Figure 17. Evolution of the size distribution in the lowest cell over 48 hours. Processes include a sea-salt surface source and surface deposition (and no mixing)

The newly injected particles in section 30 (2.4-3.1 μm dry radius), are no longer confined to the lowest cell as shown in Figure 16, but are now mixed throughout the first 400 m as seen in Figure 19. Many of the particles, initially in the upper part of the 400 m layer, are mixed down to the surface where they are subject to removal by gravitational settling. (Figures 19 and 16 have different vertical scales) The equilibrium surface concentration for Section 30 is about half the original concentration.

Figure 20 shows the evolution of the size distribution in the lowest cell over a 48 hour period when turbulence is presence. The large depletion of particles at small radii due to surface deposition seen in Figure 17 has been spread over 400 meters greatly reducing the depletion in cell 1. Likewise the large increase at intermediate sizes due to sea-salt injection into the lowest cell is spread to a greater vertical extent reducing the concentration in the lowest cell. Particles larger than about 1 μm appear to reach an equilibrium concentration that is less than the initial concentration within the 48 hour time period. The concentration of particles smaller than 1μm (and larger than the sea-salt source cutoff) keeps increasing because of the extremely long time to reach equilibrium, which is the result of the very small settling velocity. The time constant for achieving equilibrium at radii of about 1 to 3 μm inferred from Figure 20 is much faster than the actual time constant and that given in Hoppel et al. (2002). In this particular case, we fortuitously started with concentrations very near their equilibrium values in this size range as indicated by the concentration at about 1 μm radius in Figure 20 which does not change with time. The size distributions (not shown) in all cells below 500 m and at radii smaller than 5 μm

look almost identical indicating that the atmosphere is well mixed to that height. For particles larger than about 5 μm, the concentration drops off more rapidly with increasing size as the height increases, reflecting the fact that gravitational settling is sufficiently strong to establish a vertical gradient in the concentration of large particles.

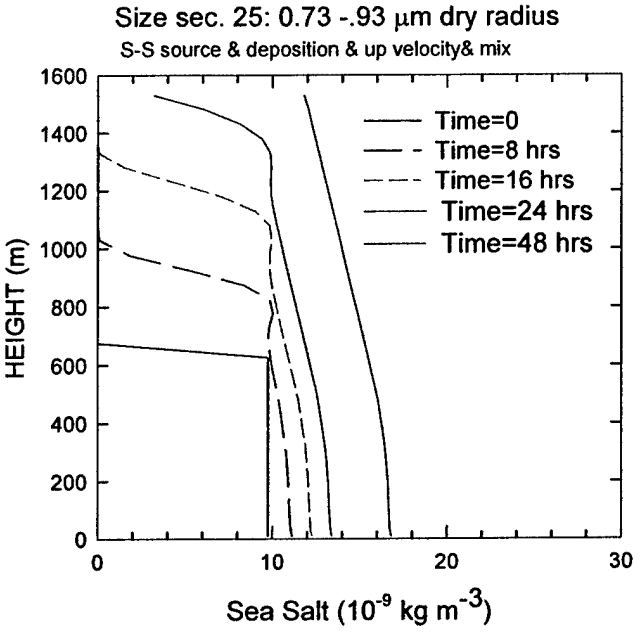

Figure 18. Change in the vertical profile in section 25 when turbulence is added. Compare with Figure 15.

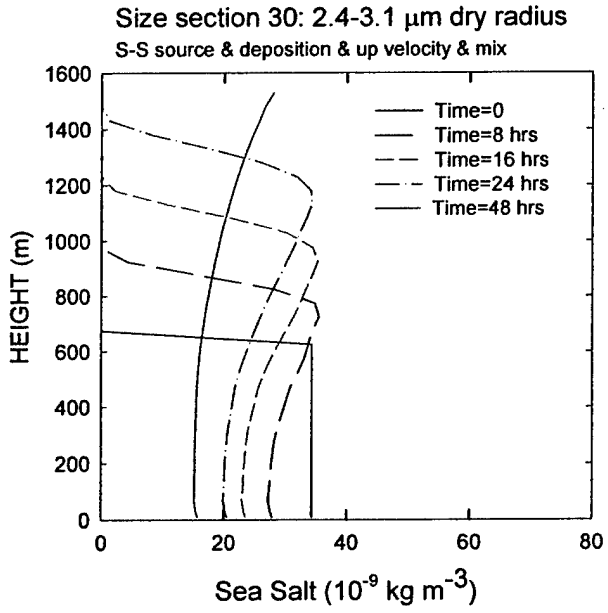

Figure 19. Change in the vertical profile in section 30 when turbulence is added. Compare with Figure 16.

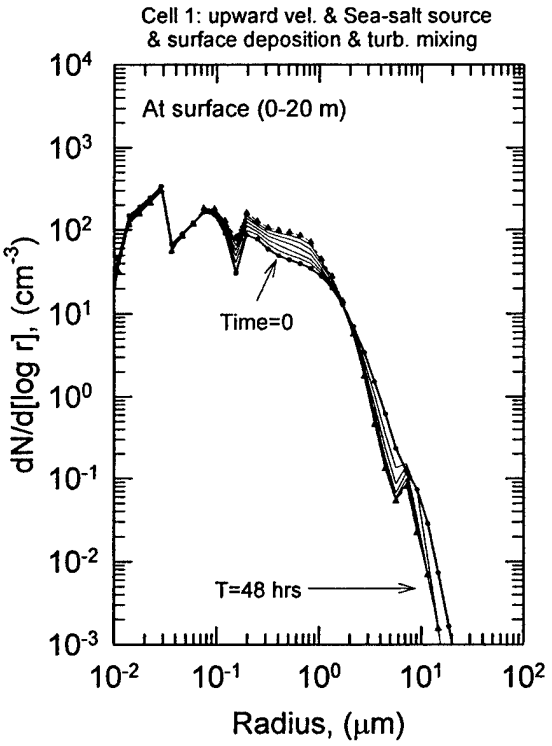

Figure 20. Evolution of the size distribution when turbulence is added. Compare with Figure 17.

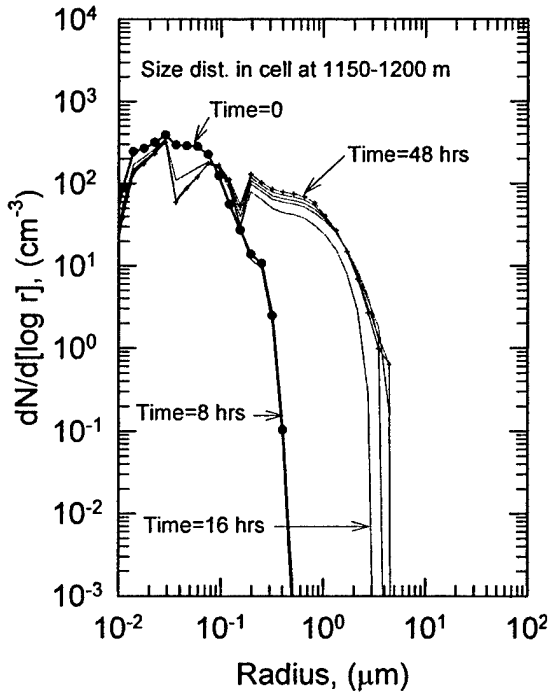

Figure 21. Evolution of the size distribution at 1150-1200 meters when turbulence is added

Figure 21 shows the evolution of the size distribution in the cell at 1150-1200 meters. At this height turbulent mixing is negligible and the size distribution remains constant for 8 hours because the air between 600 and 1150 m has the same initial size distribution. By 16 hours the air from the lower layers has reached this cell and the size distribution looks much like that in the mixed layer except for the gravitational filtering out of the largest particles.

Downward velocity. The prior solutions were for an upward directed velocity. Figure 22 shows the solution for the size distribution in the lowest cell for the case of a downward velocity with profile shown in Figure 2. The processes included are the same as the prior case shown for upward velocity in Figure 20. The interpretation of Figure 22 is quite instructive. For the first 8 hours there is no change except that caused by gravitational settling at radii greater than about 5 μm. After 8 hours subsidence brings air from above down into the mixed layer, and the size distribution at radii below about 0.1 μm approaches that of the FT at 16, 24 and 32 hours. (The initial size distribution above the mixed layer is shown in Figure 5 and again in Figure 23 as square symbols). At 40 and 48 hours subsidence has brought particles free air from above the domain into the top of the mixed layer, which causes the dilution seen at radii smaller than about 0.1 μm. At larger sizes we see continuous dilution after 8 hours, since there are no large particles in the upper air. However, the continuous injection of sea-salt particles at the surface causes equilibrium to be achieved in the mixed region. As seen in Figure 22, the time required to reach equilibrium decreases with particle radius. At 10 μm radius the equilibrium is reached in 8 hours, but requires 48 hours at 1 μm.

If we now let the air above the domain (which we will here refer to as FT air) have the same size distribution as the upper air and allow exchange, as determined by an exchange velocity, V_{ex} , we get the evolution of the size distribution shown in Figure 23. One might be surprised that the magnitude of the size distribution at small radii after 48 hours is only about half that of the FT size distribution. In the case shown in Figure 23 we have used an exchange velocity of 1 cm s^{-1}, which is the same as the downward velocity in the top cell. In steady state the flux into the top of the domain must equal the flux out of the bottom of the top cell

$$V_{ex}(QFT - Q_{Ncell}) = V_{Ncell}Q_{Ncell} \quad \text{or}$$

$$Q_{Ncell} = \frac{V_{ex}}{V_{ex} + V_{Ncell}} QFT$$

where Q_{Ncell} and QFT are the mass concentrations in the top cell and above the domain respectively. Figure 24 shows the evolution of the profile of mass in a small size section where gravitational settling is negligible. The equilibrium value is half the FT value in keeping with the above equation. The mixing below about 400 m keeps the gradient in concentration below 400 m small. To get the concentration to remain at its initial value would require that $V_{ex} >> V_{Ncell}$. (For larger particles V_{Ncell} includes gravitational settling.)

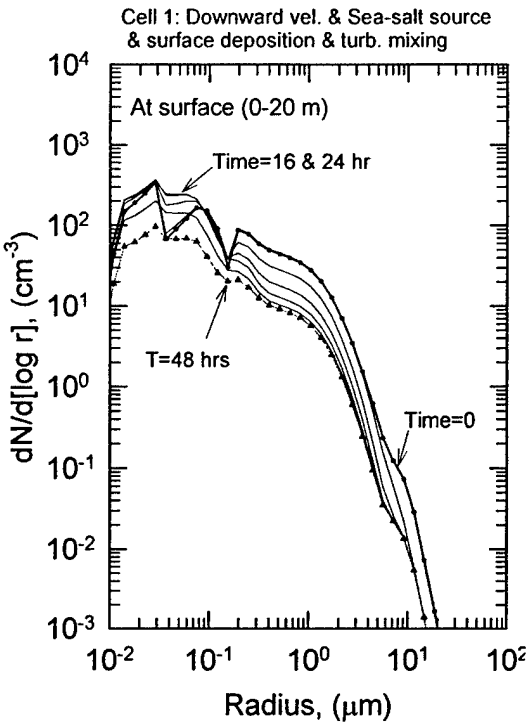

Figure 22. Evolution of the size distribution over 48 hours when the direction of the vertical velocity profile is downward. The sea-salt aerosol source, surface deposition and mixing are all on.

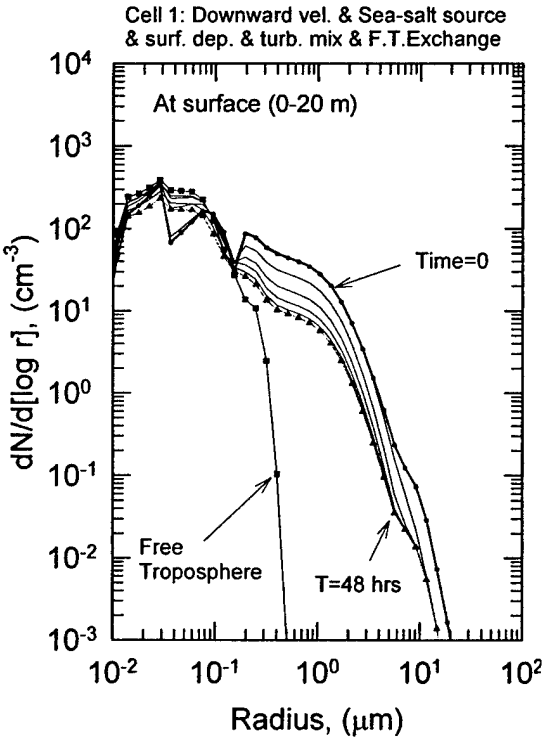

Figure 23. Same as in Figure 22 but with free troposphere exchange also turned on, where the free troposphere size distribution is shown the blue squares.

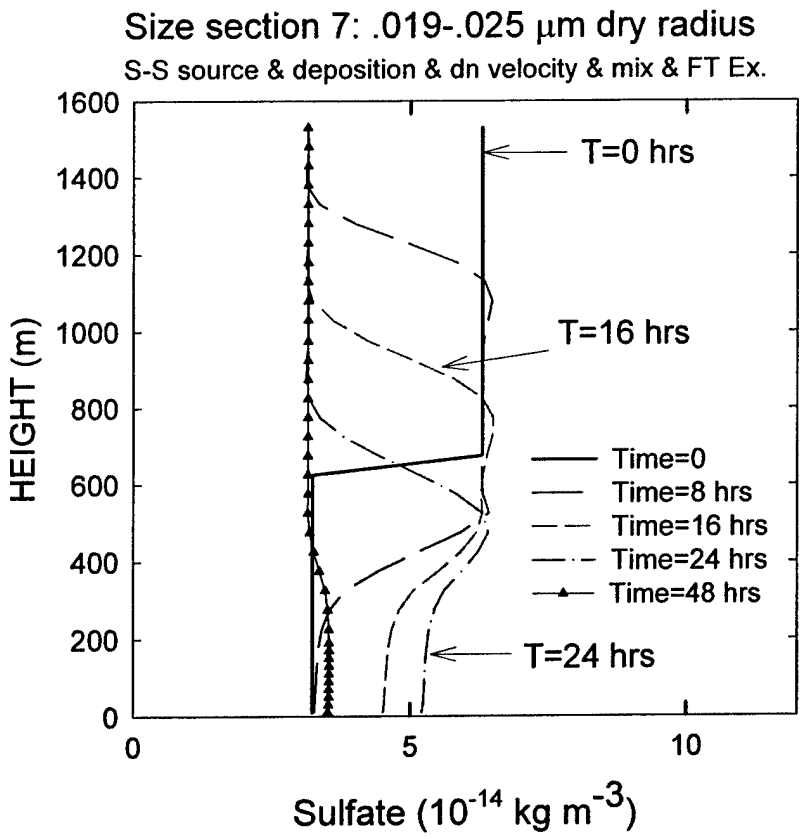

Figure 24. Time evolution of Section 7 when FT exchange is on and the exchange velocity is equal to the downward air velocity in the top cell.

The model allows the mechanism of exchange with the FT to be either through an exchange velocity as illustrated above or by a downward (subsidence) velocity into the top cell (or, as illustrated earlier, an upward velocity out of the domain). An exchange velocity is sometimes provided from experimental data (usually derived from moisture or ozone exchange).

If instead of using the exchange velocity (gradient transfer) to interact with the FT, we allow an downward airflow to bring mass in from above we get the solution shown in Figures 25-27. The downward velocity into the top cell from above is vertical air velocity plus the settling velocity for particles and just the air velocity for trace gases. For the solutions shown we have set the mass concentrations above the domain to be the values in the top cell of the domain. In this case there should be no temporal change in the concentration in the top cell. Hence, in Figure 25, subsidence causes no change in concentration in the upper cells. In the mixed layer the concentration approaches the FT concentration as subsiding air displaces the original air. Figure 25 shows that the small radius end of the size distribution approaches the FT distribution and the large salt particles mix upward, and strike a balance between the source and surface deposition of particles as before. The profile of DMS, shown in Figure 27 is interesting. There is no DMS initially below 600 m, and a low concentration above. Subsiding air brings DMS downward and the concentration decreases somewhat because of oxidation by OH. DMS is mixed upward from the surface, but DMS from the surface source cannot penetrate above 500

meters, the extent of the mixed layer. The DMS concentration in the mixed layer is, under these circumstances determined by the source at the surface, surface deposition, dilution by subsiding air from above, and loss resulting from OH oxidation.

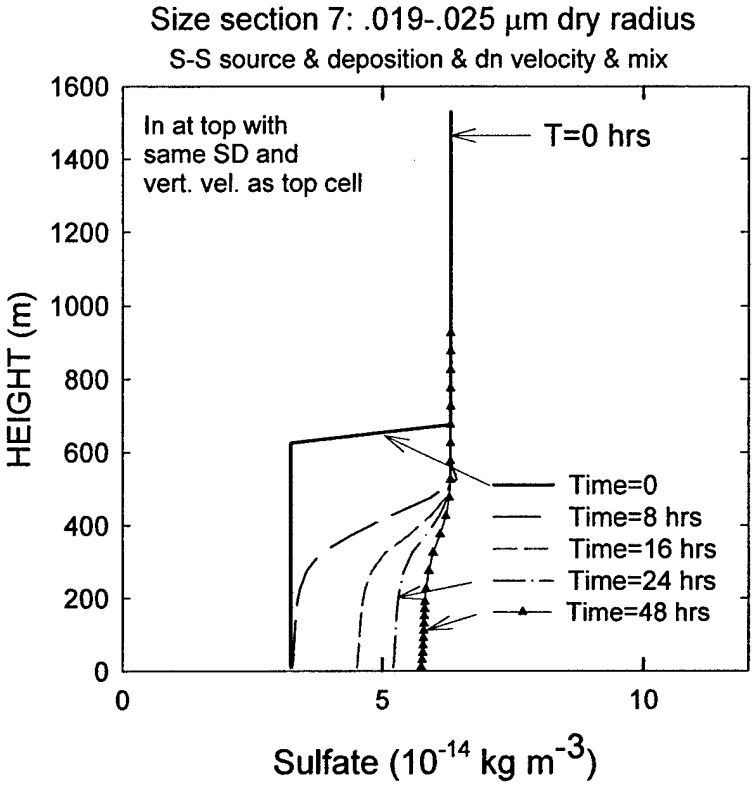

Figure 25. Same as in Figure 24 except FT exchange is turned off and material flows in from above with vertical downward velocity in the top cell.

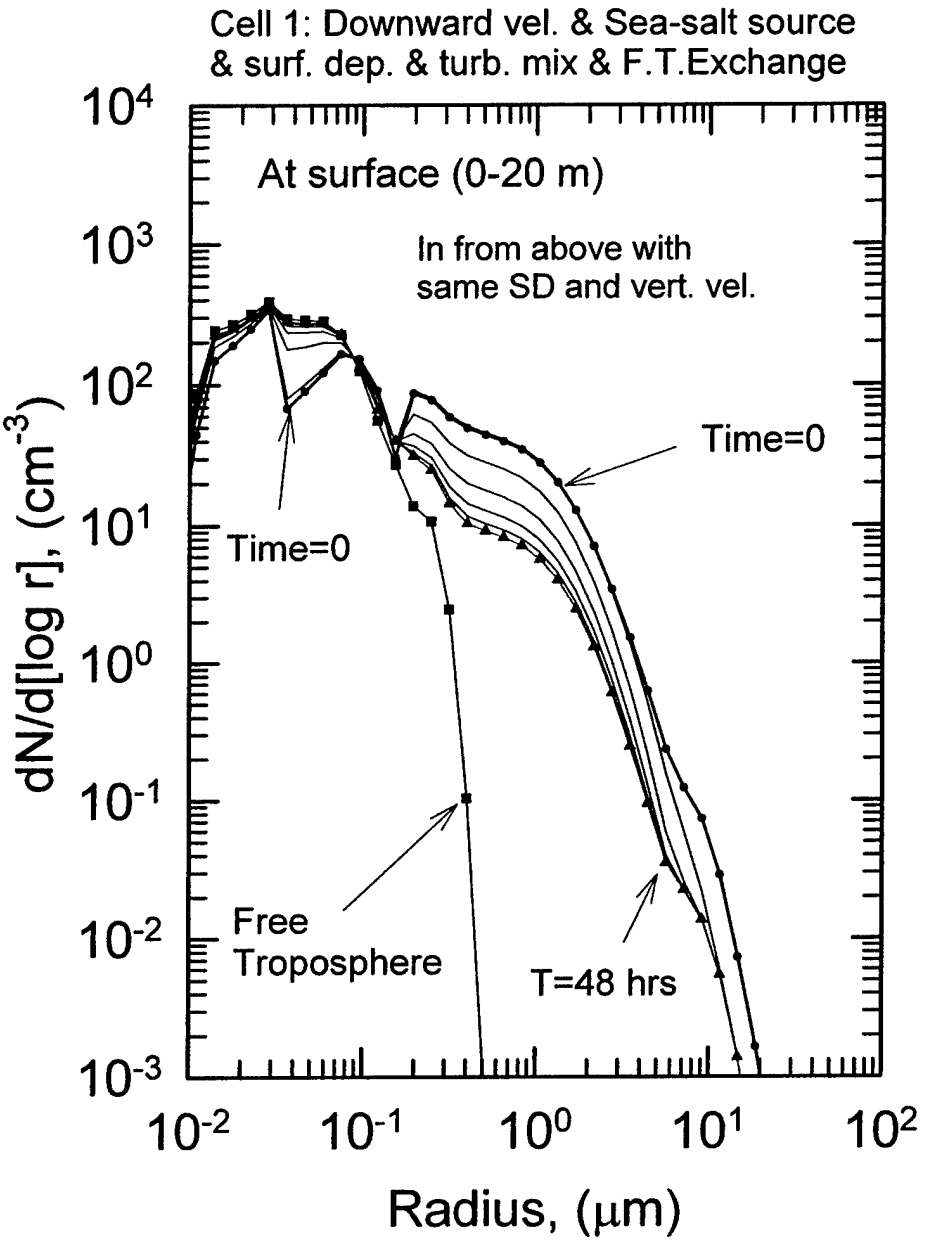

Figure 26. Evolution of the size distribution in the lowest cell when there is subsidence into the top from above. At small radii the MBL size distribution is determined by the subsiding air and at large sizes by the surface source of sea-salt aerosol.

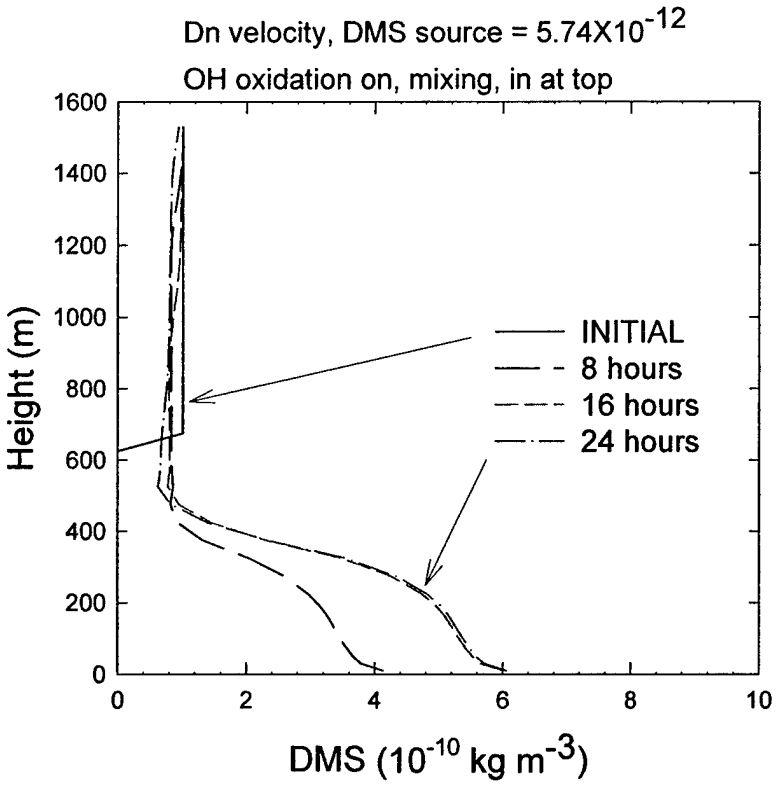

Figure 27. A small concentration of DMS is supplied from above by subsidence where the decrease in the subsiding air is due to oxidation ay OH. In the mixed layer DMS is mixed upward from the surface source.

IV. CONCLUSIONS

The above tests, plus ones not shown, demonstrate that the addition of large-scale atmospheric motions (subsidence and lifting) can be added to the NRL aerosol and trace gas model (MARBLES). The large-scale convergence and divergences that cause the vertical motion must be generated externally. The current source of the vertical velocities is the Navy's 3-D mesoscale model COAMPS (Coupled Ocean Atmosphere Meteorological Prediction System). The aerosol model is run along an air-mass trajectory generated from the output of COAMPS which also supplies all the vertical profiles of meteorological data required by the aerosol model along the trajectory (i.e.; turbulent mixing coefficients, large-scale vertical velocities, temperature, relative humidity, etc.). The 1-D aerosol model can be visualized as a Lagrangian column moving with a mean horizontal wind speed of the MBL. The 1-D limitation requires horizontal homogeneity, but the vertical stratification moves upward or downward, or is compressed or expanded by large-scale subsidence and lifting. This (1-D) limitation arises because the air that enters or leaves the column, at any designated height, must have the same aerosol load both inside and outside the column. Within any cell (horizontal layer), all the aerosol source, sinks and transformation processes, which are responsible for the evolution of the size distribution, are taking place.

The tests shown above were designed to test the algorithms and therefore do not represent realistic atmospheric conditions. Nevertheless, working through the examples will not only help one to understand how the numerical simulations work, but will also contribute to a better understanding of how atmospheric dynamics affect the vertical variations of aerosols.

For an ideal Lagrangian column there is no exchange through the walls of the column. The modifications introduced by the work reported here allow transport through the walls due to convergence and divergence of the local flow field, with the restriction, that the air entering the column at a given height has the same aerosol load inside and outside the column (this is the 1-D or horizontally-homogeneous limitation). It is clear that in regions where there are localized sources and sinks, the 1-D assumption will not be valid. It is useful to further examine the 1-D limitation and define under what conditions the 1-D assumption holds.

First consider the case of large-scale subsidence causing horizontal divergence in the MBL flow field. In this case the airflow will be out the sides of the column and horizontal inhomogeneities outside the column will not affect conditions within the column. The subsiding air will propagate downward through the top of the column and be mixed with the preexisting air by turbulent diffusion. In this case, the 1-D limitation does not appear to be significant, but the accuracy with which we can specify the flux into the top of the column is critical. The vertical variation of large sea-salt particles (radius greater than about 5 μm) will occur more rapidly than dilution by mixing so that the subsidence will have little effect on large sea-salt particles. Smaller particles, whose lifetime is much longer (determined primarily by precipitation scavenging), will be well mixed vertically and the concentration will slowly change to reflect that in the air above the MBL.

For the case of convergence within the MBL, with upward velocity in the column, horizontal-inhomogeneities outside the column can be advected into the column. Except for large sea-salt particles where the establishment of the gravitationally induced vertical gradient is more rapid than the convergence, the potential for change within the column caused by convergence is real. To further evaluate the effect of horizontal inhomogeneities during convergence consider the following situation.
(1) Consider a Lagrangian column that is being advected along an air mass trajectory. In principal, a Lagrangian column is defined such that the mean horizontal flow around the periphery is zero (except for the small amount due to local convergence). Since the model grid spacing is the order of a kilometer, we take the radius r_i of the column as 1 km. The Eulerian wind field of the mesoscale model includes the effects of the large-scale convergence. The local convergence in the Lagrangian flow field around the column is what gives rise to the vertical velocity in the column.
(2) Further consider a cylinder of radius r_o and height H_{mbl} as shown in Figure A1 coaxial with the Lagrangian column. The region inside r_o is assumed to be horizontally homogeneous. The region outside r_o is horizontally inhomogeneous and we wish to calculate the time required for the inhomogeneous region at r_o to reach the column r_i for an upward velocity u_{up} which is uniform over the upper surface at H_{mbl} , where H_{mbl} is the height of the MBL. The mean radial velocity is given by

$$v_r = \left(\frac{\pi r^2}{2\pi r H_{mbl}}\right) v_{up} = \left(\frac{r}{2H_{mbl}}\right) v_{up} \qquad \text{(A1)}$$

The time to travel from r_0 to r_i is then

$$t = \left(\frac{2H_{mbl}}{v_{up}}\right) \ln\left(r_o / r_i\right) \qquad \text{(A2)}$$

If the horizontally homogeneous region has a radius of 10 km (r_o = *10* km) and if the MBL is assumed to have a height of 1000 m with uniform lifting of 1 cm s^{-1}, then the time for the inhomogeneities to reach the column is about 5 days. This is about the same time as a mean lifetime for an aerosol particle at the (accumulation mode) radius where the maximum lifetime in the MBL occurs (Hoppel et al. [1990], Figure 24). If the time for the local convergence to advect the aerosol from the region of the inhomogeneity to the column is greater than the mean lifetime of the aerosol, then other dynamic processes already accounted for in the column can resolve the evolution of the size distribution. We know from measurements that horizontal homogeneity can extend over large areas of the ocean with more rapid changes occurring in frontal areas and near coasts (see, for example, Hoppel et al. [1990]). While the above analysis is very rough it does give us a clue as to when we would expect the Lagrangian column model, as modified here, to give representative results. *With regard to the 1-D limitation*, the model is expected to be more representative when the column is advected through regions of subsidence (high pressure regions) than regions of convergence. In regions of convergence (vertical lifting) horizontal gradients of aerosol concentrations must be weak over regions the order of 10 km around the advecting column for the 1-D approximation to be valid.

We have not mentioned horizontal mixing due to turbulence as a mechanism for transporting horizontal gradients. Estimates indicate that horizontal mixing in the Lagrangian frame over distances the order of 10 km is not as severe as the problem discussed above. Turbulent mixing has a tendency to destroy horizontal gradients.

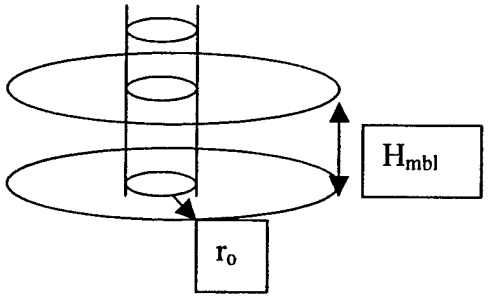

Figure 28. r_i is the radius of the Lagrangian column, r_o is the radius which divides the homogeneous from the inhomogeneous.

ACKNOWLEDGMENTS

This work was sponsored by the Office of Naval Research through the Naval Research Laboratory.

REFERENCES

Fitzgerald, J.W., W.A. Hoppel, and F. Gelbard, A one-dimensional sectional model to simulate multicomponent aerosol dynamics in the marine boundary layer. I. Model description. J. *Geophys. Res., 103*, 16085-16102, 1998a.

Fitzgerald, J.W., J.J. Marti, W.A. Hoppel, G.M. Frick and F. Gelbard, A one-dimensional sectional model to simulate multicomponent aerosol dynamics in the marine boundary layer. II. Model application. *J. Geophys. Res., 103* 16103-16117, 1998b.

Gelbard, F., J.W, Fitzgerald, W.A. Hoppel, A one-dimensional sectional model to simulate multicomponent aerosol dynamics in the marine boundary layer. III. Numerical methods and comparisons with exact solutions. *J. Geophys. Res., 103,* 16119-16132, 1998.

Hoppel W.A., J.W. Fitzgerald, G.M. Frick, and R.E. Larson, Aerosol size distributions and optical properties found in the marine boundary layer over the Atlantic Ocean. J. Geophy. Res., 95, 3659-3686, 1990.

Hoppel W.A., G.M. Frick, and J.W. Fitzgerald, Surface source function for sea-salt aerosol and aerosol dry deposition to the ocean surface. *J. Geophy. Res. 107(D19)*, ACC, 7:1-17, dio:10.1029/2001JD002014, 2002.

Hoppel W.A., P.F. Caffrey, and G.M. Frick, Particle Deposition on Water: surface source vs. Upwind Source, *J. Geophy, Res.* In press., 2005.

Monahan, E.C., D.E. Spiel, and K.L. Davidson, A model of marine aerosol generation via whitecaps and wave disruption, in *Oceanic Whitecaps and Their Role in Air-Sea Exchange Processes*, edited by E.C. Monahan and G MacNiocaill, pp. 167-174, D. Reidel, Norwell, Mass., 1986.

Smith, M.H., P.M. Park, and I.E. Consterdine, Marine aerosol concentrations and estimated fluxes over the ocean, *Q. J. Roy. Meteor. Soc., 119*, 809-824, 1993.

APPENDIX: Including the density stratification of the atmosphere.

The analysis given in this report can and should be expanded to include the density stratification of the atmosphere. Under typical atmospheric conditions the density decreases by about 10% in the first 1000 m and 18% in the lowest 2000 meters.

Let ρ be the air density, then conservation of mass requires

$$\frac{\partial \rho}{\partial t} = -\nabla \bullet \rho \vec{v}^{\,f} \qquad \text{(A1)}$$

For the purposes of calculating the density stratification, the atmosphere can be considered to be in static equilibrium $\partial\rho/\partial t = 0$.

Following the same procedure that led to Eq. (7), we obtain Eq. (A2) from (A1) for the case of a density-stratified atmosphere.

$$-\rho_t w_t A + \rho_b w_b A - \oint_{hor} \rho \vec{v}^{\,f} \bullet d\vec{S} = 0 \qquad \text{(A2)}$$

Combining Eq. (A2) and Eq. (5), we find the change of the mass in a cell to be

$$\frac{1}{A}\frac{\partial M_{cell}}{\partial t} = -\left[(w_t^f + w_t^g)m_t - (w_b^f + w_b^g)m_b\right] + \langle m \rangle \frac{(\rho_t w_t^f - \rho_b w_b^f)}{\langle \rho \rangle} \qquad \text{(A3)}$$

where $\langle \rho \rangle$ is the mean density in the cell which can be taken as the density at the center of the cell. Equation (A3) replaces Eq. (8), which was for an incompressible atmosphere. Values for ρ_t, ρ_b, and $\langle \rho \rangle$, for a given cell can be obtained from the meteorological model, sounding, or standard atmosphere as the application warrants. Equation (A3) predicts a change in aerosol (sectional) mass even if there is no velocity gradient and no aerosol mass gradient

$$\frac{1}{A}\frac{\partial M_{cell}}{\partial t} = \langle m \rangle w^f \frac{(\rho_t - \rho_b)}{\langle \rho \rangle} = \langle m \rangle w^f \delta \qquad \text{(A4)}$$

where w^f and m are constant with height, and δ is the fractional change in density across the cell.

$$\delta = \frac{\rho_t - \rho_b}{\langle \rho \rangle} \qquad \text{(A5)}$$

It may seem contradictory to have a change in the aerosol mass in a cell when the aerosol mass flux is the same at the top and bottom of the cell. However the difference in air mass flux at the top and the bottom requires an inflow of air (horizontally) given by Eq. (A4). If we want the mass in the cell to remain constant when the vertical velocity is constant with height, Eq. (A3) requires that the fractional change in the aerosol mass density be equal (and opposite) to the fractional change in the air mass density.

$$\frac{m_t - m_b}{\langle m \rangle} = \delta = \frac{\rho_t - \rho_b}{\langle \rho \rangle}$$

where we have assumed that the gravitational settling velocity does not change with height (the case with no change in relative humidity with height).